

1 **Characterization of soot produced by the Mini Inverted Soot Generator with an atmospheric simulation**  
2 **chamber**

3 *Virginia Vernocchi<sup>1,2</sup>, Marco Brunoldi<sup>1,2</sup>, Silvia G. Danelli<sup>1,2</sup>, Franco Parodi<sup>2</sup>, Paolo Prati<sup>1,2</sup>, Dario*  
4 *Massabò<sup>1,2,\*</sup>*

5  
6 <sup>1</sup>*Dipartimento di Fisica - Università di Genova, via Dodecaneso 33, 16146, Genova (Italy)*

7 <sup>2</sup>*INFN – Sezione di Genova, via Dodecaneso 33, 16146, Genova (Italy)*

8  
9 *\*Correspondence to: D. Massabò (massabo@ge.infn.it)*

10

11 **ABSTRACT**

12 The performance of a Mini-Inverted Soot Generator (MISG) has been investigated at ChAMBRé (Chamber  
13 for Aerosol Modelling and Bio-aerosol Research) by studying the properties of soot particles generated by  
14 ethylene and propane combustion. This work deepens and expands the existing characterization of the MISG  
15 also exploiting an atmospheric simulation chamber (ASC). Differently from previous works, MISG  
16 performance has been also tested at different fuel flows and higher global equivalence ratios. MISG exhausts  
17 were investigated after their injection inside the atmospheric simulation chamber: this is another novelty of  
18 this work. Starting from an extensive classification of combustion conditions and resulting flame shapes, the  
19 MISG exhaust was characterized in terms of concentration of emitted particles and gases, particle size  
20 distribution and optical properties. Soot particles were also collected on quartz fibre filters and then analysed  
21 by optical and thermal-optical techniques, to measure the spectral dependence of the absorption coefficient  
22  $b_{abs}$ , and their composition in terms of Elemental and Organic Carbon (EC and OC). Significant differences  
23 could be observed when the MISG is fuelled with ethylene and propane in terms of particle size: in particular,  
24 the production of super-micrometric aggregates was observed for ethylene combustion. With equal combustion  
25 conditions, ethylene produced higher number concentration of particles and smaller mode diameters. Soot  
26 particles produced by propane combustion resulted in higher EC:TC ratios and they were more light absorbing  
27 than particles generated by ethylene combustion. Values of the Mass Absorption Cross Section (MAC) and of  
28 the Angstrom Absorption Exponent (AAE) turned out to be compatible with the literature, even if with some  
29 specific differences. The comprehensive characterization of the MISG soot particles is an important piece of  
30 information to design and perform experiments in atmospheric simulation chambers. Particles with well-  
31 known properties can be used, for example, to investigate the possible interactions between soot and other  
32 atmospheric pollutants, the effects of meteorological variables on soot properties and the oxidative and  
33 toxicological potential of soot particles.

34 **1. Introduction**

35 “Soot” refers to combustion-generated carbonaceous particles that are a by-product of incomplete  
36 combustion of fossil fuels and/or biomass burning (Nordmann et al., 2013; Moore et al., 2014). When  
37 investigated by optical techniques, soot particles are generally referred as Black Carbon, BC (Petzold et al.  
38 2013) while the result of thermal - optical characterizations is referred as Elemental Carbon, EC, (Bond and  
39 Bergstrom, 2006). However, both BC and EC are defined in operative terms that do not identify the same  
40 compounds (Massabò and Prati, 2021) and often produce non-negligible differences in concentration values.

41 Soot particles constitute an important fraction of anthropogenic particulate matter (PM) especially in urban  
42 environments (Weijer et al. 2011), and are emitted by traffic, domestic stoves, industrial chimneys and by any  
43 incomplete combustion process. Several works state adverse effects of soot both on climate (Ackerman et al.,  
44 2000; Menon et al., 2002; Quinn et al., 2008; Ramanathan and Carmichael, 2008; Bond et al., 2013) and health  
45 (Pope et al., 2002; Anenberg et al., 2010; Gan et al., 2011; Cassee et al., 2013; Lelieveld et al., 2015). From  
46 the climatic point of view, soot particles absorb the solar radiation, causing a positive radiative forcing: BC is

47 considered one of the most significant radiative forcing agent, second only to CO<sub>2</sub> (Ramanathan and  
48 Carmichael, 2008; Bond et al., 2013). Another positive effect on radiative forcing is related to the darkening  
49 of glaciers surface due to the deposition of BC (Skiles et al., 2018). Soot contributes to air pollution also via  
50 reactions with several gas species, as NO<sub>2</sub>, SO<sub>2</sub> and O<sub>3</sub> (Finlayson-Pitts and Pitts, 2000; Nienow and Roberts,  
51 2006). Effects on health include cardiopulmonary morbidity and mortality (Janssen et al., 2012). Soot particles  
52 are suspected to be particularly hazardous to human health, because they are sufficiently small to penetrate the  
53 membranes of the respiratory tract and enter the blood circulation or be transported along olfactory nerves into  
54 the brain (Nemmar et al., 2002; Oberdörster et al., 2005). The understanding of properties and behaviour of  
55 soot particles when they are suspended in the atmosphere is thus necessary to fully assess their adverse effects  
56 and the use of proxies with controlled and known properties can be useful. In this context, soot generators are  
57 employed as stable sources of soot particles. So far, soot generators have been employed for studies on optical  
58 properties (Zhang et al. 2008; Cross et al. 2010; Mamakos et al. 2013; Utry et al. 2014 b; Bescond et al. 2016),  
59 instruments calibration (Onasch et al. 2012; Durdina et al. 2016) and several other purposes, such as studies  
60 on atmospheric processing of soot particles, characterization of uncoated/coated and fresh/denuded of soot  
61 particles (Pagels et al. 2009; Henning et al. 2012; Ghazi et al. 2013; Ghazi and Olfert 2013; Hu et al., 2021).  
62 The Inverted-Flame Burner (Stipe et al. 2005) is often considered as an ideal soot source (Moallemi et al.,  
63 2019 and references therein), due to its capacity to generate almost pure-EC particles and for the stability of  
64 the flame and of its exhaust (Stipe et al. 2005). To such category belongs the Mini-Inverted Soot Generator,  
65 MISG (Argonaut Scientific Corp., Edmonton, AB, Canada, Model MISG-2), used in this work.

66 The MISG can be operated with different fuels: ethylene (Kazemimanesh et al., 2019), propane (Moallemi  
67 et al., 2019, Bischof et al, 2019), and theoretically also with ethane or fuel blends with methane and nitrogen,  
68 even if, to our knowledge, no literature is available on such configurations. The air to fuel flow ratio can be  
69 adjusted to control concentration and size of the generated particles. The maximum reachable concentration  
70 declared by the manufacturer is about 10<sup>7</sup> particles cm<sup>-3</sup>, while particle size ranges from few tens to few  
71 hundreds of nm.

72 The behaviour of soot particles can be efficiently studied in/by ASCs: these are exploratory platforms which  
73 allow to study atmospheric processes under controlled conditions, that can be maintained for periods long  
74 enough to reproduce realistic environments and to study interactions among their constituents (Finlayson -  
75 Pitts and Pitts, 2000; Becker, 2006). ASC experiments are the best compromise between laboratory and field  
76 experiments, since they simulate quasi-real situations but without the uncertainties and variability of typical  
77 field measurements. Recent examples of ASC applications concern the investigation of the optical properties  
78 of mineral dust (Caponi et al., 2017) and wood-burning exhausts (Kumar et al., 2018, Hu et al., 2021).

79 Coupling the MISG to an ASC makes possible systematic experiments on the properties of soot particles  
80 exposed and maintained in different conditions. In this work, we mainly investigated the differences between  
81 MISG exhausts produced by ethylene and propane burning. Differently from previous works (Bischof et al.,  
82 2019; Kazemimanesh et al., 2019; Moallemi et al., 2019), the MISG has been connected directly to an  
83 atmospheric simulation chamber; performance has been tested also at different fuel flows and higher global  
84 equivalence ratios. The present characterization deepens and expands the existing knowledge on particles and  
85 gases produced by this soot generator. The comprehensive characterization of the MISG soot particles is an  
86 important piece of information to design the subsequent experiments. Well-characterized soot particles could  
87 be used to investigate the effects that atmospheric parameters can have on soot particles, and to study the  
88 interactions between soot particles and other pollutants.

## 89 **2. Materials and methods**

### 90 **2.1 Mini-Inverted Soot Generator**

91 The MISG, introduced by Kazemimanesh (2019), is a combustion-based soot generator working as an  
92 inverted-flame burner (Stipe et al., 2005) where air and fuel flow in an opposite direction to the buoyancy force

93 of the hot exhaust gases. The resulting co-flow diffusion flame is more stable thanks to a reduced flickering of  
94 flame tip (Kirchstetter & Novakov, 2007; Stipe et al., 2005) and consequently the soot particle generation is  
95 more stable.

96 The MISG is fed with air and fuel supplied by specific cylinders: we used both ethylene and propane, two  
97 fuels with a well-known capability of producing soot (Kazemimanesh et al., 2019; Moallemi et al., 2019). Air  
98 and fuel flow rates are controlled by two mass flow controllers (MFCs, Bronkhorst High-Tech B.V., Ruurlo,  
99 Netherlands, Models F-201CV-10K-MGD-22-V and FG-201CV-MGD-22-V-AA-000, respectively) operated  
100 via a home-made National Instruments Labview code. The air and fuel flows can be controlled in the range 0-  
101 12 lpm (i.e., litres per minute) and 0-200 mlpm (i.e., millilitres per minute), respectively. Differently from  
102 other commercial generators, the MISG does not require a third gas (i.e., N<sub>2</sub>) used as a carrier (quenching gas)  
103 and the air flow is internally split between combustion and dilution of exhaust product. This implies that the  
104 ratio of comburent and carrier gas is not controllable, and the user can only adjust the comburent to fuel ratio.

105 The efficiency of the combustion process can be given in terms of the global equivalence ratio that is the  
106 ratio between actual and stoichiometric fuel-to-air ratio:

107  
108  
109

$$110 \quad \varphi = \frac{(m_F / m_A)}{(m_F / m_A)_{st}} \quad \text{Eq.1}$$

111  
112  
113  
114  
115

where:

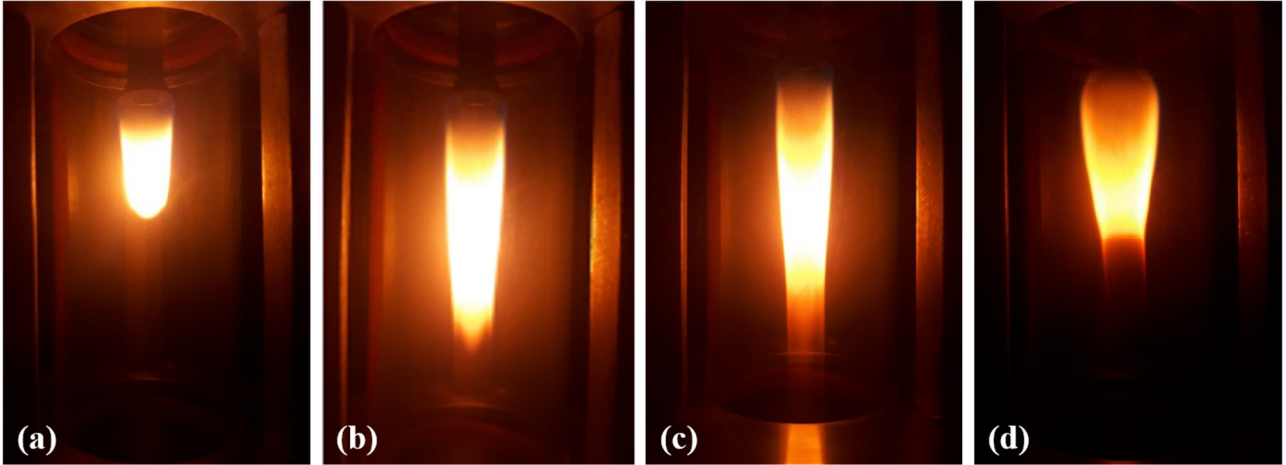
- 113 (m<sub>F</sub>/m<sub>A</sub>): actual fuel-to-air ratio;
- 114 (m<sub>F</sub>/m<sub>A</sub>)<sub>st</sub>: stoichiometric fuel-to-air ratio.

116 The fuel-to-air ratio is calculated as the opposite of the air-to-fuel ratio (AFR) that is the ratio between air and  
117 fuel masses. The stoichiometric AFR value is 15.64 (inverse value = 0.064) and 14.75 (inverse value = 0.068),  
118 for propane and ethylene, respectively.

119 The flame is classified as fuel-rich and fuel-lean when  $\phi > 1$  and  $\phi < 1$ , respectively. Mamakos (2013) reported  
120 that low fuel-to-air ratios (i.e.,  $\phi < 1$ ) generate particles with a large fraction of EC while semi-volatile organics  
121 are generated by high fuel-to-air ratios (i.e.,  $\phi > 1$ ). In this work, fuel-lean conditions were investigated only.

122 Since the combustion process can produce flame shapes having different characteristics, we first explored  
123 the range of combustion flows from 2 to 10 lpm, in 0.5 lpm steps, and from 30 to 100 mlpm, in 5 mlpm steps,  
124 respectively for air and fuel. Flame types can be distinguished (Kazemimanesh et al., 2019; Moallemi et al.,  
125 2019) as:

- 126 - *Closed tip* flame (Fig. 1.a), which generates low concentrations of soot particles (i.e., around 10<sup>3</sup> # cm<sup>-3</sup>),  
127 generally forming particle aggregates at the fuel tube nozzle.
- 128 - *Partially Open tip* flame (Fig. 1.b), the transition between *Open* and *Closed tip*.
- 129 - *Open tip* flame (Fig. 1.c), which generates high concentrations of soot particles (i.e., > 10<sup>5</sup> # cm<sup>-3</sup>).
- 130 - *Asymmetric* flame, which shows a large variability (very short, flickering, etc) and can form particle  
131 aggregates at the fuel tube nozzle.
- 132 - *Curled Base* flame (Fig. 1.d), a particular shape of the asymmetric flames that can also form particles  
133 aggregates at the fuel tube nozzle.



134

135 *Figure 1: Examples of different flame shapes: (a) Closed tip, (b) Open tip, (c) Partially Open tip, (d) Curled base flame.*

136 By the flames observation, we selected the more interesting combustion conditions (i.e., *Open tip* flames)  
 137 to perform the characterization experiments. We focused on *Open tip* flames because it is the flame that  
 138 generates higher concentrations of soot particles. Operative conditions selected for propane and ethylene  
 139 combustion are reported in Tables 1 and 2: we maintained the same air flow and global equivalence ratio with  
 140 both the fuels.

141

*Table 1: Combustion parameters and flame shapes selected for propane.*

PROPANE			
AIR flow [lpm]	FUEL flow [mlpm]	Global Equivalence Ratio	Flame shape
7	70	0.244	Partially Open Tip
7	75	0.261	Open Tip
7	80	0.278	Open Tip
7	85	0.296	Open Tip
8	70	0.213	Partially Open Tip
8	75	0.228	Open Tip
8	80	0.244	Open Tip
8	85	0.259	Open Tip

142

143

144

145

Table 2: Combustion parameters and flame shapes selected for ethylene.

<b>ETHYLENE</b>			
<b>AIR flow</b>	<b>FUEL flow</b>	<b>Global Equivalence Ratio</b>	<b>Flame shape</b>
<b>[lpm]</b>	<b>[mlpm]</b>		
7	118	0.244	Partially Open Tip
7	127	0.261	Open Tip
7	135	0.278	Open Tip
7	144	0.296	Open Tip
8	118	0.213	Partially Open Tip
8	127	0.228	Open Tip
8	135	0.244	Open Tip
8	144	0.259	Open Tip

147

148

149

## 2.2 Chamber setup

150

151

152

153

154

155

156

157

158

159

160

161

162

163

164

165

166

167

168

169

170

171

172

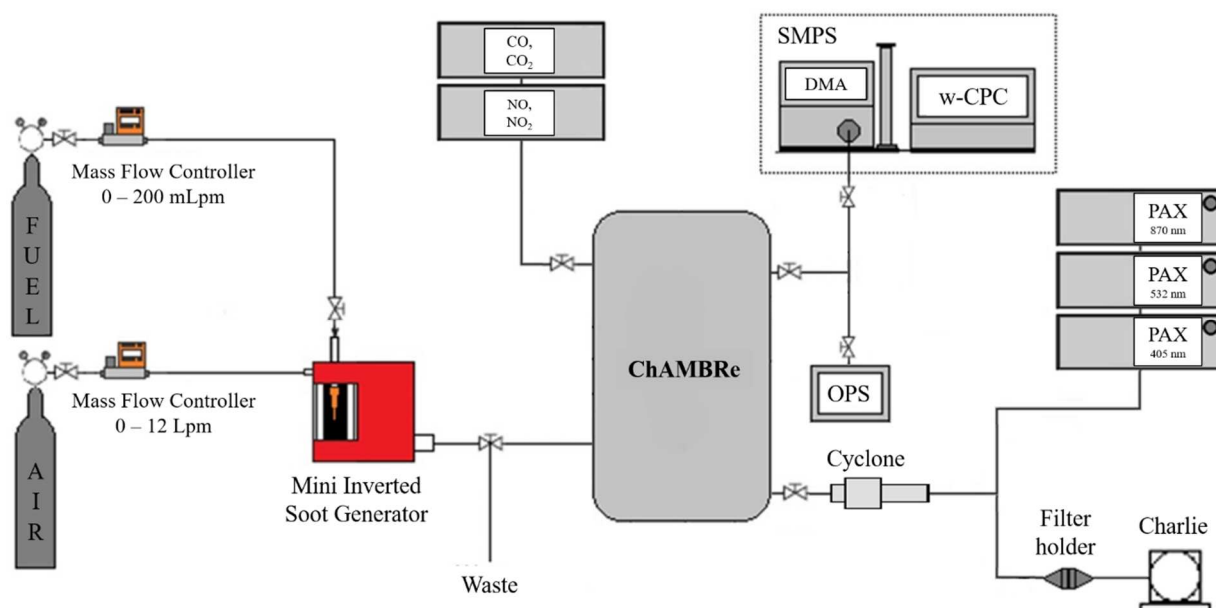
Experiments took place at the ChAMBRé (Chamber for Aerosol Modelling and Bio-aerosol Research) facility (Massabò et al., 2018; Danelli et al., 2021) located at the Physics Department of the University of Genoa.

ChAMBRé is a stainless-steel chamber, with a volume of about 2.2 m<sup>3</sup>. Inside the chamber, relative humidity, temperature, and pressure are continuously monitored by a HMT334 Vaisala® Humicap® transmitter and a MKS Instruments 910 DualTrans™ transducer, respectively. Two gas analyzers from Environnement SA, continuously monitored the concentration of NO/NO<sub>2</sub> (model: AC32e), and CO/CO<sub>2</sub> (model: CO12e) inside the chamber or, alternatively, in the laboratory. The mixing of gas and aerosol species is favoured by a fan installed in the bottom of the chamber: mixing time for gaseous species is of about 180 s with a fan rotating speed of 1.6 revolutions per second. A composite pumping system (rotary pump TRIVAC® D65B, Leybold Vacuum, root pump RUVAC WAU 251, Leybold Vacuum and Leybold Turbovac 1000) allows to evacuate the internal volume down to 10<sup>-5</sup> mbar; in this way ChAMBRé is cleaned before each experiment. Before and during the experiments, ambient air enters the chamber throughout a 5-stage filtering/purifying inlet (including a HEPA filter, model: PFIHE842, NW25/40 Inlet/Outlet – 25/55 SCFM, 99.97 % efficient at 0.3 µm). The whole set-up is managed by a custom NI Labview SCADA (Supervisory Control And Data Acquisition).

The layout of the experimental configuration adopted for the MISG characterization is shown in Fig. 2.

The MISG was warmed for about 45 minutes before injecting soot particles inside the chamber. Injection of soot particles inside ChAMBRé lasted 2 or 3 minutes, depending on the soot concentration required for each experiment. We performed some fluid dynamic evaluations with the Particle Loss Calculator software tool (PLC; von der Weiden et al., 2009). The connection between MISG and ChAMBRé was made by Swagelok adaptors (size ¾”) and ISO-K flanges (16 mm diameter) to avoid any possible leak; the length of the line was 65 cm. The geometry of our experimental setup, combined with particle size and used flow rates, resulted in

173 particle losses lower than 0.1 % in the dimensional range of 80-2000 nm. All the experiments were performed  
174 at atmospheric pressure,  $19^{\circ} < T < 21^{\circ} \text{C}$  and  $\text{R.H.} < 50 \%$ .  
175



176  
177 *Figure 2: Layout of the MISG set-up at ChAMBRé.*

### 178 2.3 Size distribution measurements

179 Particle concentration and size distribution inside the chamber were measured by a scanning mobility  
180 particle sizer (SMPS, TSI Inc., Shoreview, MN, USA, Model 3938), composed by a differential mobility  
181 analyzer (DMA, TSI Inc., Shoreview, MN, USA, Model 3081A) and a water condensation particle counter  
182 (w-CPC, TSI Inc., Shoreview, MN, USA, Model 3789). The water-CPC is filled using technical demineralized  
183 water (Conductivity (20°C), max. 1.5  $\mu\text{S}/\text{cm}$ ; VWR Chemicals INTERNATIONAL S.R.L.). The SMPS was  
184 set to measure particles with mobility diameter from 34 nm to 649 nm; aerosol sample and sheath airflow rates  
185 were fixed at 0.17 lpm and 1.60 lpm, respectively, while the scanning period for each cycle was 70 s. The  
186 DMA unit integrates an impactor with an orifice of 0.0508 cm, resulting in cut-off capability at 50 % of 940  
187 nm, useful to exclude all the particles larger than this size to enter in the column. Frequent cleaning of this part  
188 was necessary to ensure proper operation and avoid clogging; at the end of each experiment, the whole  
189 impactor system was cleaned using compressed air and isopropyl alcohol.

190 We corrected diffusion losses in the instrument by using the option included in the instrument software;  
191 size distributions were not corrected for multiple charges effects through the TSI proprietary software (Aerosol  
192 Instrument Manager, Version 11-0-1). An example of comparison between size distribution corrected and  
193 uncorrected by the multiple charge correction algorithm is shown in the Supplementary (see Fig. S.1).

194 Among the other chamber instruments, an Optical Particle Sizer (OPS, TSI Inc., Shoreview, MN, USA,  
195 Model 3330) was used for short times to spot the particle size distribution in the range 0.3-10  $\mu\text{m}$ .

### 196 2.4 Online optical measurements

197 Three photoacoustic extinction-meters (PAXs, Droplet Measurement Technologies, Boulder, CO, USA)  
198 were deployed, providing the online determination of the soot particles absorption coefficients at  $\lambda = 870, 532$

199 and 405 nm. PAXs are constituted by a measurement cell where aerosol optical properties are measured by  
200 two different mechanisms (<https://www.dropletmeasurement.com/> PAX Operator Manual). The sample flow  
201 rate (1 lpm) is split in two different sectors of the cell, both crossed at the same time by the light of a modulated  
202 laser diode. In the absorption sector, soot particles absorb light and release acoustic waves, which are then  
203 detected by an ultra-sensitive microphone. The intensity of the acoustic signal is interpreted to infer the particle  
204 absorption coefficient. In the other sector, a wide-angle reciprocal nephelometer measures the scattering  
205 coefficient instead. It is noteworthy that no correction for the truncation angle is applied by the manufacturer:  
206 this can lead to substantial underestimation of the scattering coefficient, which generally grows as the particle  
207 size increases and the single scattering albedo (SSA) approaches unity. Few papers in literature deal with the  
208 correction for truncation errors in nephelometer measurements (Bond et al., 2009, Modini et al, 2021) for  
209 highly absorbing particles: little is known on the dependency of scattering phase function on the particle  
210 morphology and how this might impact truncation. However, since particles produced by soot generators have  
211 dimensions generally lower than 1  $\mu\text{m}$  and SSA values lower than 0.3 (Moallemi et al., 2019), we disregarded  
212 this issue. At the time of the experiments, the three PAXs had been just calibrated by the manufacturer.

213 In some experiments, soot concentration inside the chamber was too high to be measured directly by PAXs;  
214 and a diluter (eDiluter Pro, Dekati Ltd., Kangasala, Finland) was deployed. Dry air from a cylinder was merged  
215 prior to the PAXs inlet with dilution factor 1:100. Tests performed with and without the diluter demonstrated  
216 a substantial reproducibility of the optical properties measured by the PAXs when the proper dilution factor is  
217 considered.

## 218 **2.5 Offline analysis**

219 Soot particles were also collected on pre-fired 47 mm diameter quartz fibre filters (Pallflex Tissuquartz  
220 2500 QAO-UP) held in a stainless-steel filter holder to allow additional offline analysis. The sampling started  
221 when stable gas and particle concentration values were reached inside the chamber (i.e., about 3 minutes -  
222 corresponding to the chamber mixing time - after the MISG switching off): for each working condition three  
223 filters with different loadings were obtained by a low-volume sampler (TECORA – Charlie HV) working at a  
224 fixed sampling flow (i.e., 10 lpm during experiments without cyclone and 13.67 lpm during experiments with  
225 cyclone).

226 For each sample, the EC and OC mass concentration was determined by thermal-optical transmittance  
227 analysis (TOT) using a Sunlab Sunset EC/OC analyzer and the NIOSH5040 protocol (NIOSH, 1999),  
228 corrected for temperature offsets. We also performed some tests adding a backup filter during the sampling to  
229 determine the volatile fraction of OC.

230 Prior to EC/OC determination, particle-loaded filters were analyzed by the Multi-Wavelength Absorbance  
231 Analyzer (MWAA, Massabò et al., 2013 and 2015), a laboratory instrument for the offline direct quantification  
232 of the aerosol absorption coefficients at five different wavelengths ( $\lambda = 850, 635, 532, 405$  and  $375$  nm). Such  
233 features have been previously exploited in the frame of several field campaigns in urban and rural sites (Scerri  
234 et al., 2018; Massabo et al, 2019; Massabo et al, 2020; Moschos et al., 2021), as well as in remote sites  
235 (Massabo et al., 2016; Saturno et al., 2017; Baccolo et al., 2021).

## 236 **2.6 Cyclone experiments**

237 Soot aggregates are also generated by the MISG. Kazemimanesh (2019) retrieved super-aggregates larger  
238 than 2  $\mu\text{m}$  for ethylene combustion while Moallemi (2019) showed aggregate structures larger than 1  $\mu\text{m}$  with  
239 propane. On this basis, confirmed by some short checks by the OPS, we replicated each experiment (see Sect.  
240 2.1) both without and with a cyclone (PM1 Sharp Cut Cyclone - SCC 2.229, MesaLabs, Lakewood, CO, USA)  
241 inserted upstream the PAXs and filters sampler (Fig. 2). The cyclone has a cut-off of 1  $\mu\text{m}$  at a nominal flow  
242 of 16.66 lpm.

## 243 **3. Results and Discussion**

### 244 **3.1 Characterization tests**

245 The categories of flame shape observed in the range of air and fuel flows discussed in sect. 2.1.2 are  
246 summarized in Supplementary (see Tables S.1 and S.2), for propane and ethylene respectively. The MISG  
247 characterization with propane has been previously published (Moallemi et al., 2019) and we used it as a  
248 reference. Fuel flows higher than 85 mlpm were not investigated due to instrumental limitation. A similar  
249 characterization with ethylene also exists but it only partly covers the flow ranges explored in the present work.  
250 We got some differences especially in the transition range to *Open tip* flames, probably due to the different  
251 setups. In addition, the subjectivity of the visual determination, that is user dependent, can lead to differences.  
252 It is noteworthy that no correlation could be found between the global equivalence ratio ( $\phi$ ) and the shape of  
253 the corresponding flame. This means that the fundamental parameter of the combustion process can not be  
254 used to predict the flame shape.

255 The repeatability and stability of the MISG emissions were investigated for all the combustion conditions  
256 listed in Table 1 and 2, in terms of number concentration and size distribution of the generated soot particles.  
257 Different combustion conditions were selected, and four experiments were performed for each combination of  
258 air and fuel flows. We chose to keep fixed the air flow to observe the differences produced by different fuel  
259 flows that correspond to different flame shapes (i.e., *Partially Open tip* or *Open tip*). In each test, we recorded  
260 the values of total particle number concentration, peak concentration, and mode diameter. The repeatability  
261 was calculated as the percentage ratio between standard deviation and mean value (i.e., the relative standard  
262 deviation) of identical repeated experiments. With propane, mode reproducibility turned out to be 6 %, while  
263 total concentration and peak concentration showed a 16 % repeatability. With ethylene, the repeatability was  
264 4 % and 10 %, respectively for mode and total/peak concentration. In addition, we monitored the combustion  
265 gases: CO<sub>2</sub> and NO concentration varied by about 2 % and 3 %, respectively with propane and ethylene.

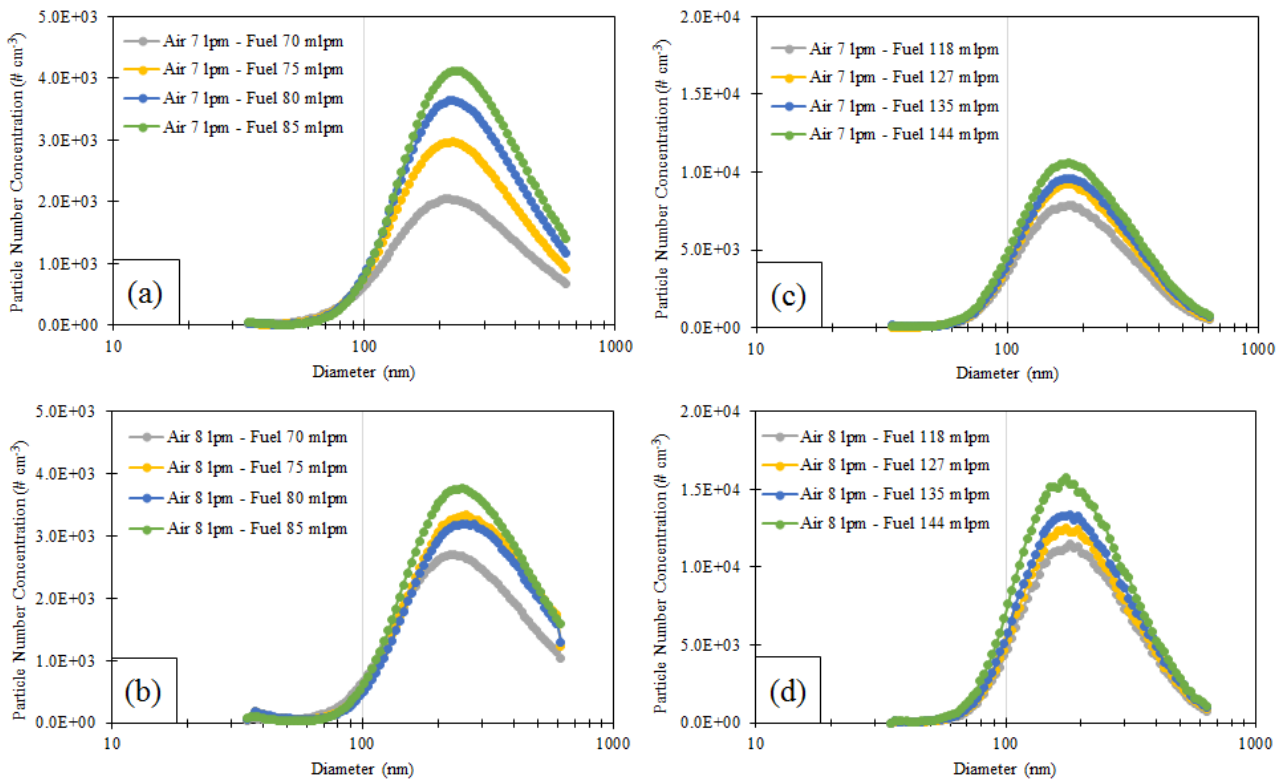
### 266 **3.2 Comparison between propane and ethylene exhausts**

267 Previous works investigated the exhausts of MISG fuelled by ethylene (Kazemimanesh et al., 2019) and  
268 propane (Moallemi et al., 2019). We expand here to a detailed comparison between the two fuels, focusing on  
269 ASC experiments. In addition, we reproduced some of the conditions investigated in the previous works  
270 obtaining a good agreement for the mode diameter and SSA figures (see §3 in Supplementary for details).

#### 271 **3.2.1 Size distribution**

272 The mean size distributions observed at ChAMBre are given in Fig. 3, for all the selected operative  
273 conditions. Data were acquired starting 3 minutes (i.e., after the chamber mixing time) after the MISG  
274 switching off, for a specific time interval (i.e., 4 to 10 minutes). All the curves are normalized to the same  
275 injection time (i.e., 3 min of injection inside the chamber).





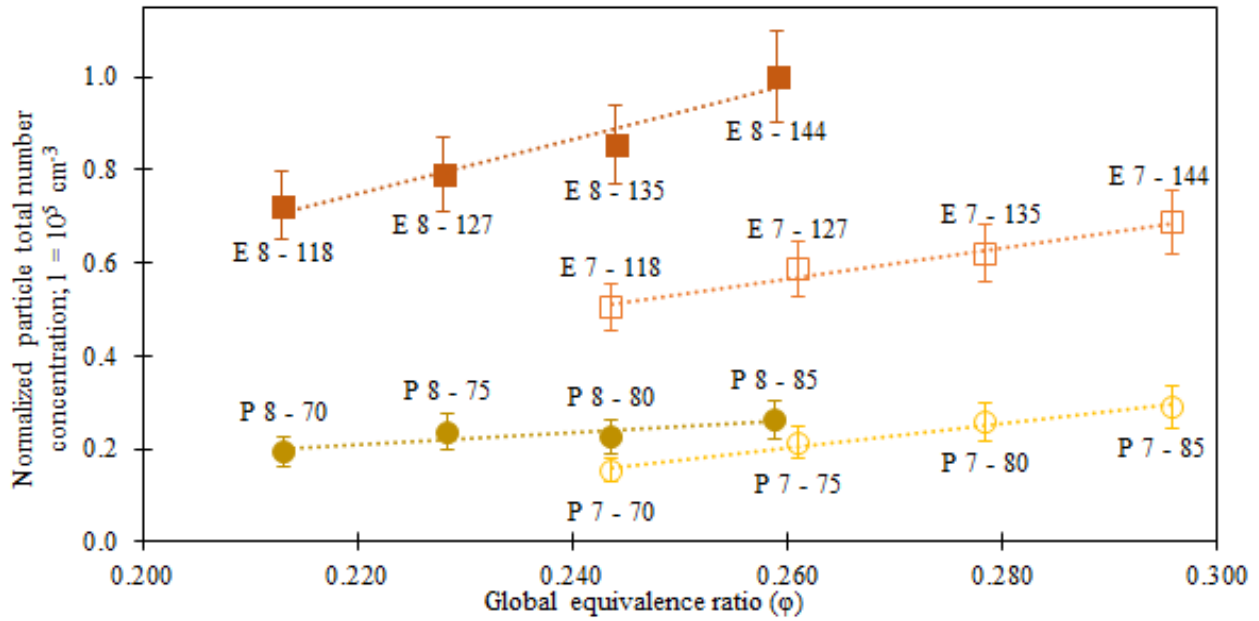
276

277 *Figure 3: Mean size distributions measured by SMPS. MISG was fuelled with propane (a) and (b) panels and ethylene*  
 278 *(c) and (d) with the air and fuel flows indicated in the plots frame.*

279 For a better comparison of different experiments, particle concentration values were normalized to the  
 280 maximum recorded in the whole set of tests and therefore varied in the 0-1 range. Fig. 4 shows the result for  
 281 the total particle number concentration. We can notice that:

- 282 - At fixed air flow, the particle number concentration increases with the fuel flow (i.e., with the global  
 283 equivalence ratio).
- 284 - In the same combustion conditions (i.e., same air flow and same global equivalence ratio), ethylene generates  
 285 more particles than propane.
- 286 - With ethylene and at fixed fuel flow, the particle number concentration increases with the air flow. The same  
 287 holds in some cases with propane but with much smaller variations.

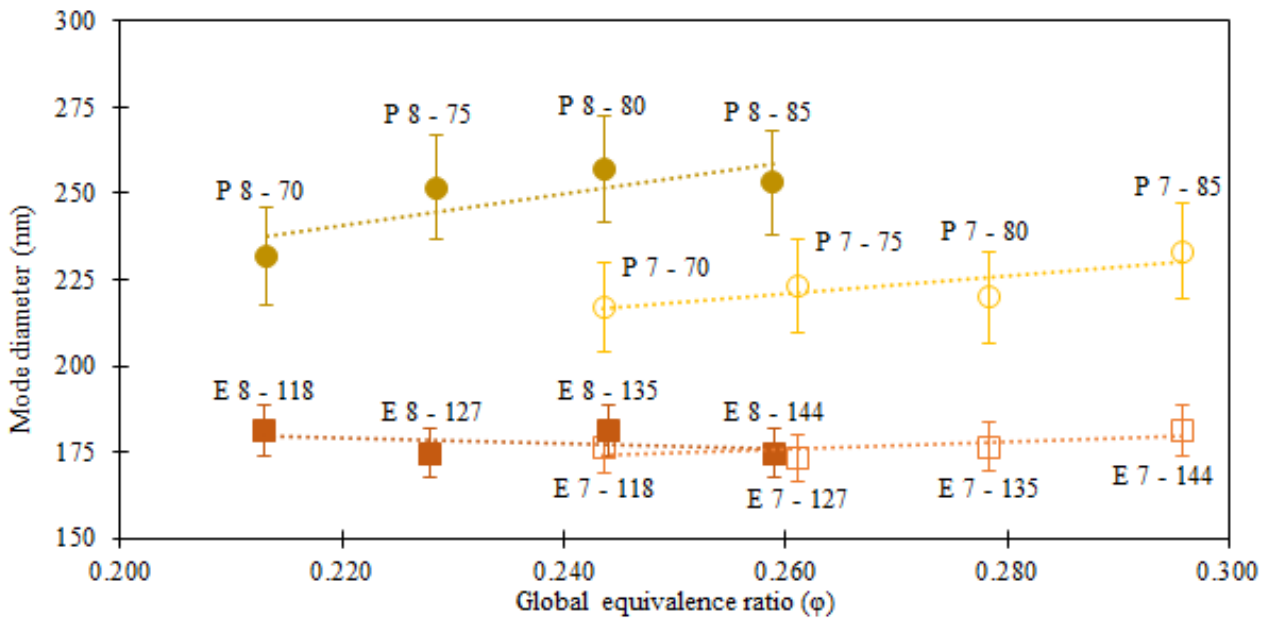
288



289

290 *Figure 4: Particle number concentration vs the global equivalence ratio. Values are normalized to the highest of the*  
 291 *whole set. Each point is labelled by E or P (ethylene or propane) and a pair of numbers indicating air and fuel flow*  
 292 *rate, respectively in lpm and mlpm. Dotted lines aim to facilitate the reader eye.*

293 A similar comparison is shown in Fig. 5 for the particle mode diameter: while the values are basically constant for ethylene,  
 294 for propane, the mode diameter slightly increases with air flow (at fixed fuel flow). Furthermore,  
 295 at each  $\phi$  value, propane generated particles bigger than ethylene.



296

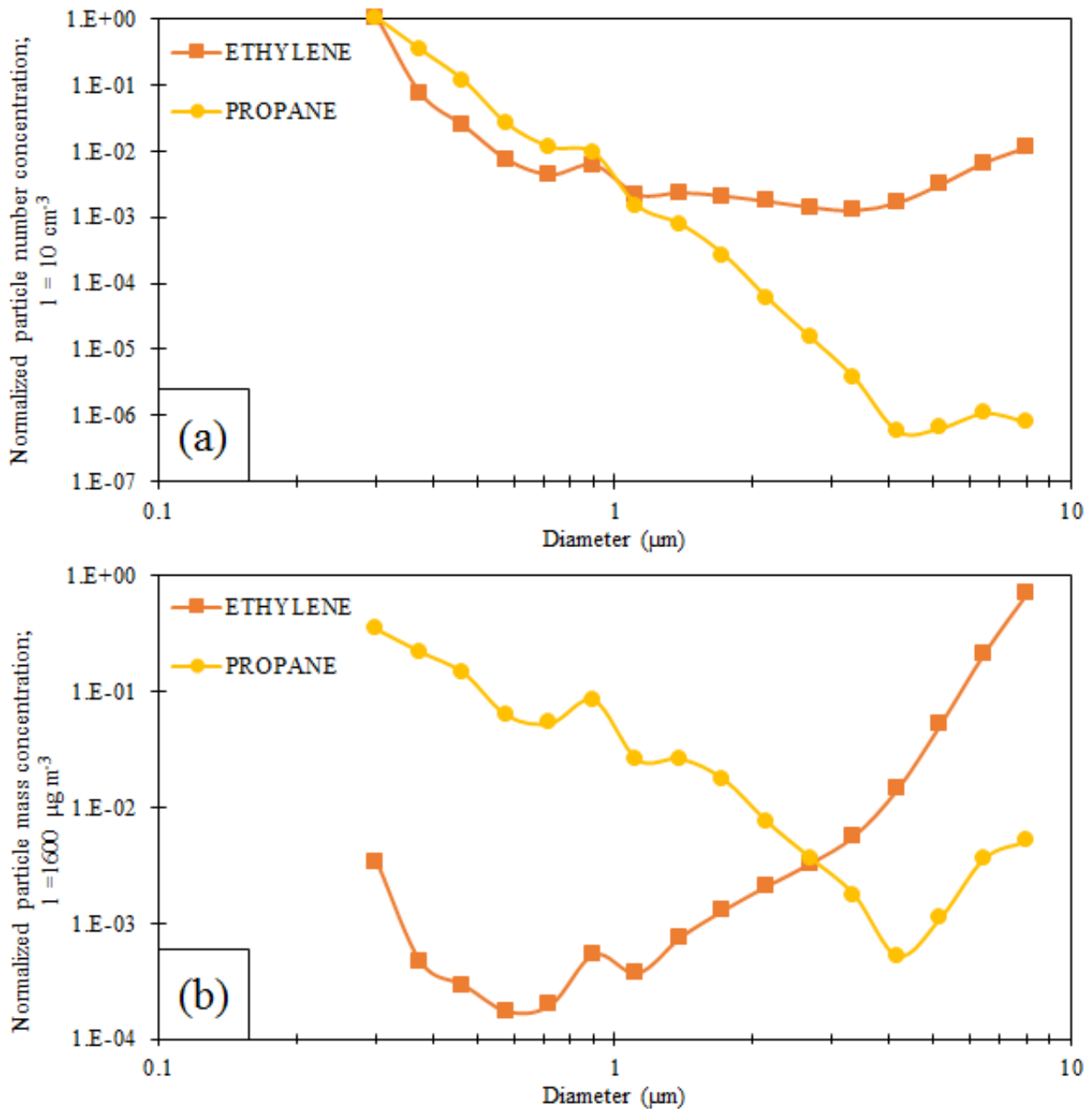
297 *Figure 5: Mode diameter versus the global equivalence ratio. Each point is indicated by E or P (ethylene or propane)*  
 298 *and a pair of numbers indicating air and fuel flow rate, respectively in lpm and mlpm. Dotted lines aim to facilitate the*  
 299 *reader eye.*

300 Even if the direct comparison between our findings and results from previous works (Bischof et al., 2019;  
 301 Kazemimanesh et al., 2019; and Moallemi et al., 2019) are not directly comparable (since feeding flows and  
 302 global equivalence ratios are different), some similarities can be identified. Previous works observed that by

303 increasing the fuel flow, the particle number concentration increases too, that is in agreement with what we  
304 observed for both the fuels. In addition, Bischof (2019) reported that with propane the particle mode diameter  
305 did not depend on the global equivalence ratio; we observed this behaviour for ethylene instead.  
306 Kazemimanesh (2019) showed a clear increase in mode diameter, corresponding to an increase of fuel flow  
307 rate, that reached a quite constant value (i.e., around 240-270 nm) for ethylene. This trend differs from our  
308 observations, since the mode diameter in our case turned out to be quite stable at about 175 nm independently  
309 on feeding flows. This difference is probably due to the global equivalence ratios used: while in  
310 (Kazemimanesh et al., 2019) global equivalence ratios are lower than 0.206, in our case they are higher than  
311 0.213. In (Moallemi et al., 2019), instead, they observed an opposite behaviour for mode diameters: they  
312 retrieved that at fixed fuel flow, a higher air flow produced a slight decrease of the mode diameter. Both  
313 (Moallemi et al., 2019) and (Bischof et al., 2019) measured mode diameters < 200 nm, but they used different  
314 combustion conditions (i.e., lower global equivalence ratios resulting from higher air flow or lower fuel flow).  
315 We can conclude that, as expected, global equivalence ratio is the principal parameter affecting size  
316 distributions of soot particles.

317 Significant differences between the two fuels emerge when considering the super-micrometric range  
318 measured by the OPS: ethylene combustion produced a number of big particles, likely super-aggregates,  
319 probably formed in the stagnation plane at the bottom part of the combustion cell (Chakrabarty et al., 2012).  
320 This hypothesis was confirmed by dedicated experiments with the setup specifically modified in respect to the  
321 basic one (see Supplementary Fig. S.2). Kazemimanesh (2019) also observed the formation of aggregates,  
322 even with smaller dimensions (i.e., about 2  $\mu\text{m}$  of maximum Feret diameter). The particle number  
323 concentration, normalized to the total particle number concentration, is shown in Fig. 6.a. We calculated the  
324 super-micrometric fraction of the total number concentration measured by the OPS with both the fuels (Fig.  
325 6.a): this resulted to be about 3% with ethylene and 0.2% with propane. Particles larger than 4  $\mu\text{m}$  (i.e., optical  
326 equivalent diameter) were about 2% with ethylene and totally negligible with propane. Considering the particle  
327 mass distribution (see Fig. 6.b), the difference is enhanced: the super-micrometric fraction is about 99% of the  
328 total mass concentration with ethylene and 9% only with propane. Particles larger than 4  $\mu\text{m}$  contribute to the  
329 total mass (and hence to the soot concentration) for about 98% and 1%, respectively with ethylene and propane.

330 Anyway, super-aggregates formation by ethylene combustion can be partly reduced by using lower air and  
331 fuel flow rates (see Supplementary Fig. S.3 for example).



332

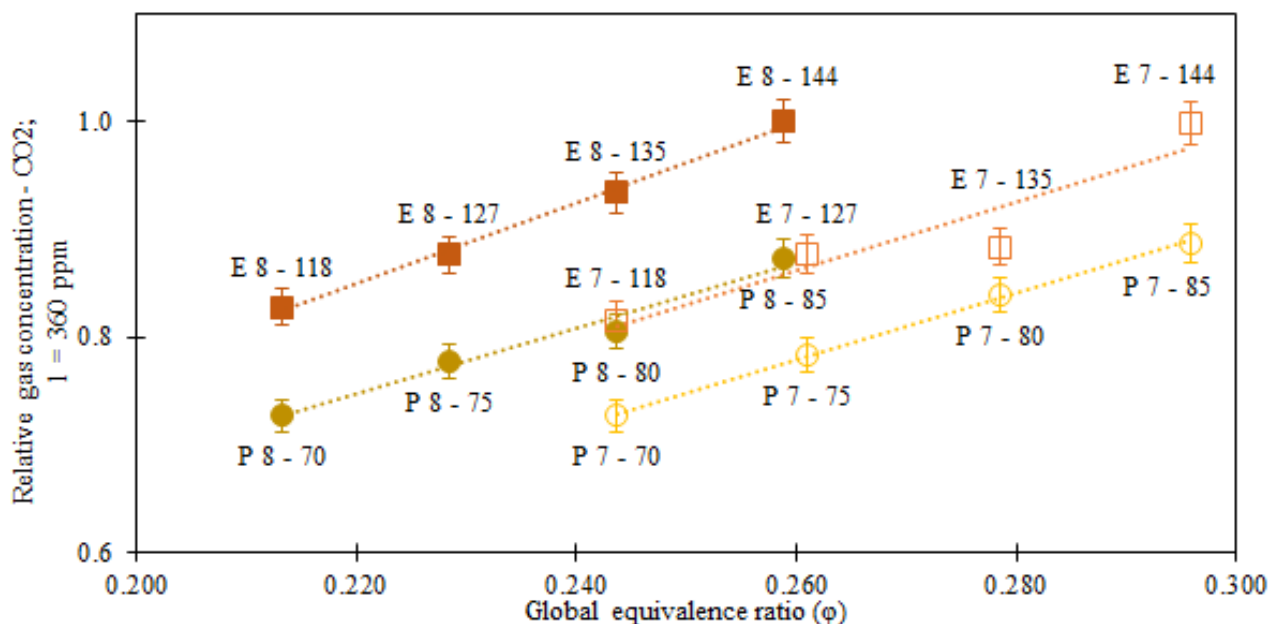
333 *Figure 6: Particle concentration normalized to the total vs. particle diameter, measured by OPS, panel (a) shows number*  
 334 *distribution, panel (b) shows mass distribution. MISG was fuelled with 7 lpm of air and 75 mlpm of fuel during propane*  
 335 *experiment and 127 mlpm of fuel during ethylene experiment. No cyclone used.*

336

### 3.2.2 Gaseous exhaust

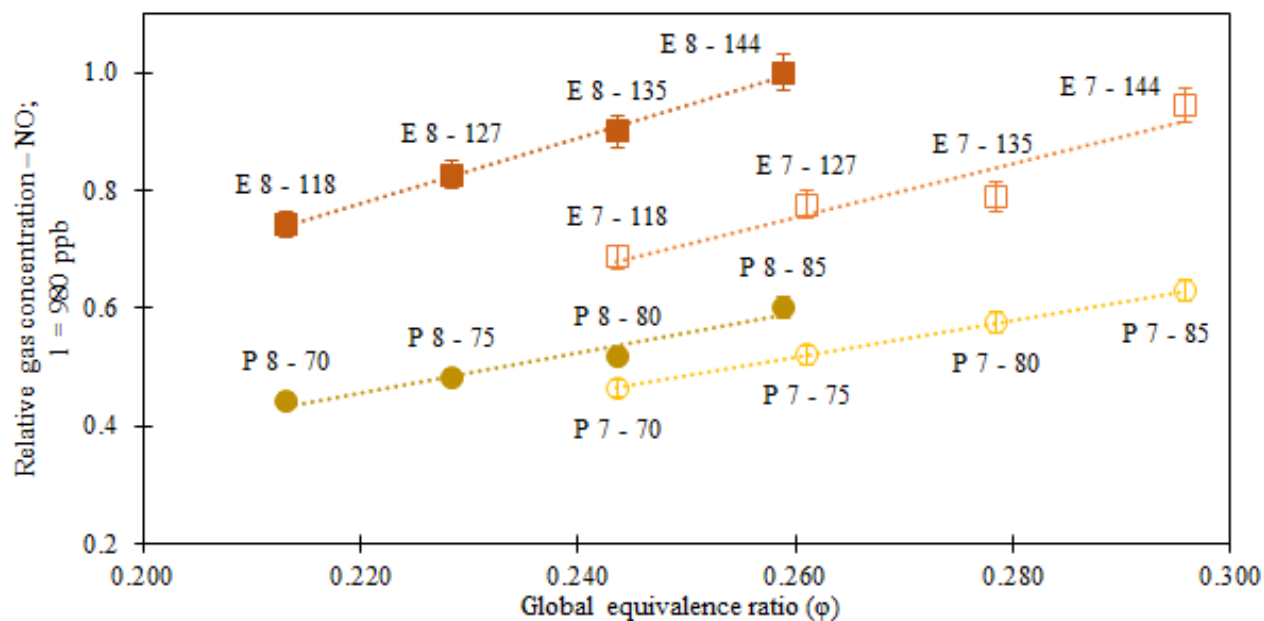
337 Gaseous emissions were characterized too, focusing on the most abundant gases i.e.,  $\text{CO}_2$  and  $\text{NO}$ . The  
 338 pattern is similar for both the gases: at fixed air flow rate, gas concentration increased with the fuel flow while  
 339 no significant differences emerged at fixed fuel flow rate and changing the air flow. At equal operative  
 340 conditions (i.e., same combustion conditions, injection time and time from the injection), gaseous emissions  
 341 were higher with ethylene than with propane. With the same normalization introduced in Fig. 3, the  $\text{CO}_2$  and  
 342  $\text{NO}$  production are compared in Fig. 7 and 8 for each selected MISG configuration. Maximum values were  
 343 360 ppm and 980 ppb, respectively for  $\text{CO}_2$  and  $\text{NO}$ , after 3 minutes of soot injection.

344



345

346 *Figure 7: CO<sub>2</sub> concentration versus the global equivalence ratio. Each value was normalized to the highest of the whole*  
 347 *set. Data points are labelled by E or P (ethylene or propane) and a pair of numbers indicating air and fuel flow,*  
 348 *respectively in lpm and mlpm. Dotted lines aim to facilitate the reader eye.*



349

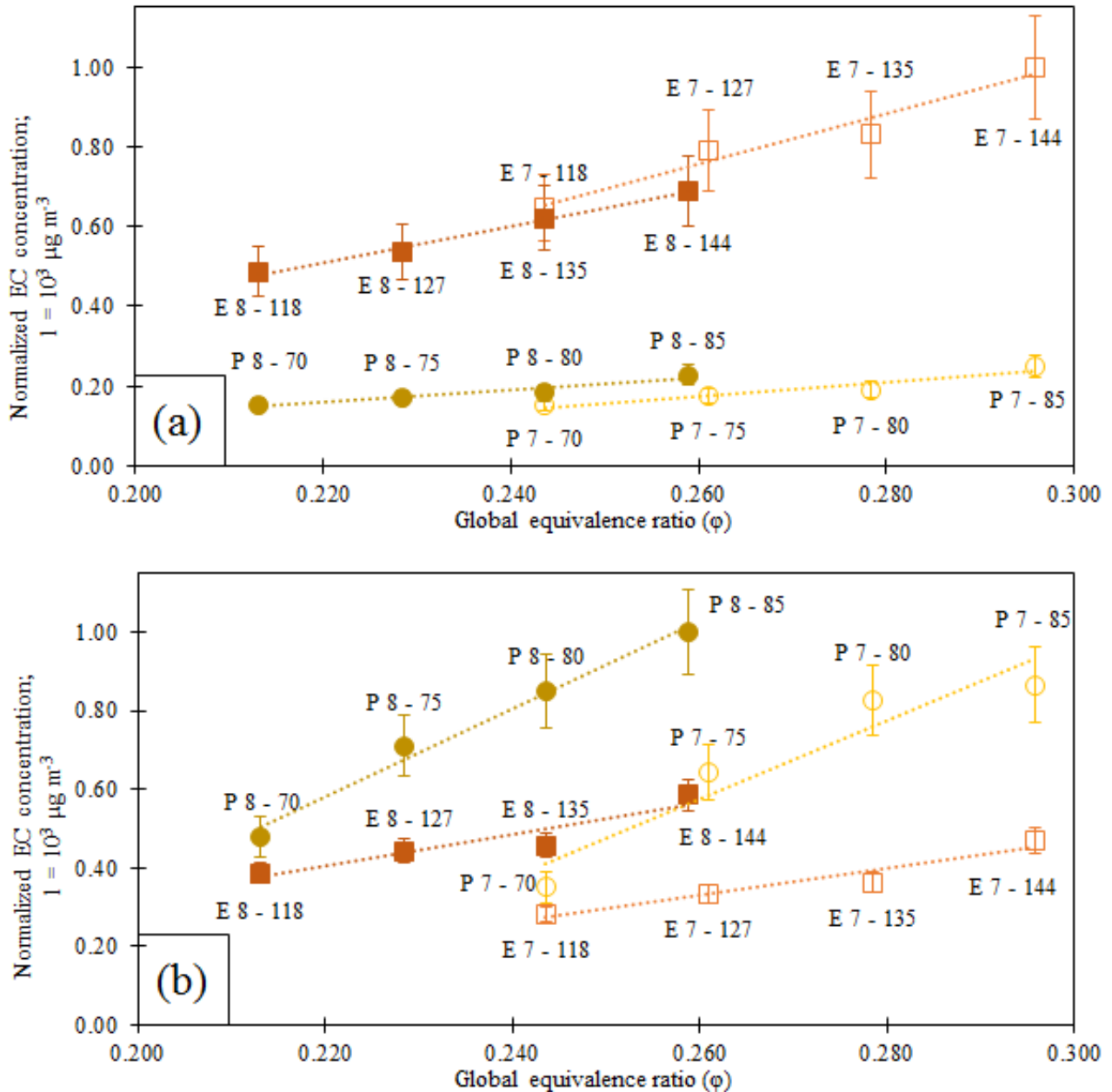
350 *Figure 8: NO concentration versus the global equivalence ratio. Each value was normalized to the highest of the whole*  
 351 *set. Data points are labelled by E or P (ethylene or propane) and a pair of numbers indicating air and fuel flow,*  
 352 *respectively in lpm and mlpm. Dotted lines aim to facilitate the reader eye.*

353

### 3.2.3 EC/OC quantification

354 The OC/EC composition was quantified by thermal-optical analysis of samples collected on quartz fibre  
 355 filters during each experiment. EC:TC concentration ratios resulted to be around 0.7 and 0.9 with propane and  
 356 ethylene, respectively. In addition, the EC:TC concentration ratios increased with the global equivalence ratio.

357 All the results are given in Fig. 9a and 9b, for experiments without and with cyclone, respectively, adopting  
 358 the same normalization already introduced in Fig. 3. When removing large particles (see Sect 3.2.1), the EC:TC  
 359 concentration ratio resulted higher with propane (0.83 against 0.79 measured with ethylene). It is worthy to  
 360 note that with ethylene about 40 % of the EC concentration was associated with particles larger than 1  $\mu\text{m}$ .  
 361 With both fuels, EC:OC ratios increase with the global equivalence ratios whether the cyclone is present or  
 362 not, in agreement with (Kazemimanesh et al., 2019) and (Moallemi et al., 2019).



363

364 Figure 9: EC mass concentration versus the global equivalence ratio, each value was normalized to the highest of the  
 365 whole set. Each point is labelled by E or P (ethylene or propane) and a pair of numbers indicating air and fuel flow rate,  
 366 respectively in lpm and mlpm. (a): no cyclone; (b) cyclone upstream the filter. Dotted lines aim to facilitate the reader  
 367 eye.

368 The OC:TC ratio varies from 0.27 for propane to 0.11 for ethylene, without cyclone and 0.20 for ethylene  
 369 to 0.16 for propane, when the cyclone was used. In each series of experiments (i.e., air flow rate 7 or 8 lpm,  
 370 ethylene or propane) the OC fraction turned out to be inversely proportional to the fuel flow with a minimum

371 at the lowest fuel flow (i.e., 70 lpm with propane and 118 lpm with ethylene). This is likely due to the shape  
372 of the flame: flames generated by the lowest fuel flow conditions are *Partially Open tip*, with less capability  
373 to generate soot particles and hence EC; so that the EC:TC ratio results lower.

374 We also performed some tests to determine the volatile fraction of OC. The OC concentration values  
375 measured on backup filters showed high variability, but they were compatible with those on not-sampled  
376 filters. We analysed 13 blank filters from different bunches and the average concentration of OC resulted  
377  $\langle \text{OC} \rangle = 0.5 \pm 0.2 \mu\text{g cm}^{-2}$  while OC concentration on backup filters was  $\langle \text{OC}_{\text{BF}} \rangle = 0.6 \pm 0.2 \mu\text{g cm}^{-2}$ . Since  
378 the average OC concentration on the corresponding main filters was  $1.4 \pm 0.7 \mu\text{g cm}^{-2}$  and the average EC  
379 concentration collected on this subset of filter was  $12.3 \pm 0.2 \mu\text{g cm}^{-2}$ , the volatile fraction phase can be  
380 considered negligible. A relationship between OC concentration on the backup filter and the global equivalence  
381 ratio was instead reported in (Kazemimanesh et al., 2019). Actually, in that study the range of investigated  
382 global equivalence ratio values was  $0.129 < \phi < 0.186$  to be compared  $\phi > 0.210$  adopted in this work.

383

### 384 3.2.4 Optical properties

385 The optical properties of the MISG aerosol were determined in terms of the absorption coefficient ( $b_{\text{abs}}$ ;  
386 i.e. the absorbance per unit length) (Massabò and Prati, 2021). The  $b_{\text{abs}}$  definition applies both to  
387 measurements directly performed on the aerosol dispersed in the atmosphere (by PAXs, in this work) and to  
388 off-line analyses on aerosol sampled on filters (by MWAA, in this work), provided a proper data reduction is  
389 adopted (Massabò and Prati, 2021; and references therein).

390 The online measured  $b_{\text{abs}}$  values were normalized to the total particle number concentration inside  
391 ChAMBRé reached in each single experiment. At each wavelength, the  $b_{\text{abs}}$  values did not show any  
392 dependence on the global equivalence ratio, with the propane producing particles more absorbent than ethylene  
393 (see Supplementary Fig. S.4 and S.5, for the experiments without and with cyclone, respectively). Similar  
394 results were obtained even for experiments without cyclone and for the  $b_{\text{abs}}$  values measured by the MWAA.  
395 Optical properties such as absorption depend on several parameters, mainly composition, mixing state, aging,  
396 and size. Considering all the experiments reported in this work, no differences in composition can be expected,  
397 since only EC particles were present: this means that differences in absorption cannot depend on particle  
398 composition. Also mixing state and aging cannot explain this difference: soot inside the chamber was fresh.  
399 We can explain the higher light absorbing capability of propane by considering differences in: size distributions  
400 (see Figs. 3-5) and morphology/density of the particles produced by the burning of the two different fuels.

401 In the literature, only data for the IR-PAX in terms of Single Scattering Albedo (SSA) for propane soot are  
402 reported. SSA(IR) values, measured during propane experiments, in our work varied from 0.15 to 0.18, in  
403 agreement with those obtained by (Moallemi et al., 2019), which ranged from 0.15 to 0.25.

404 The  $b_{\text{abs}}$  values, together with the EC concentration measured on the filter sampled during each single  
405 experiment, can be used to retrieve the Mass Absorption Coefficient (MAC) of the produced aerosol, through  
406 the relation:

$$407 \quad b_{\text{abs}}(\lambda) = \text{MAC} * [\text{EC}] \quad \text{Eq. 2}$$

408 where:

409  $b_{\text{abs}}$  [ $\text{Mm}^{-1}$ ]: absorption coefficient

410 MAC [ $\text{m}^2 \text{g}^{-1}$ ]: Mass Absorption Coefficient

411 EC [ $\mu\text{g m}^{-3}$ ]: Elemental Carbon concentration

412 The  $b_{\text{abs}}$  values were calculated directly online by the PAXs and offline by the MWAA analysis,  
413 performed at five wavelengths on the sampled filters (see Sect. 2.5). This gave the possibility to extend the  
414 characterization of the MISG and to compare two optical analyses on the same carbonaceous aerosol. Since  
415 experiments were repeated with two different setups (i.e., with and without the cyclone) and two different fuels

416 (propane and ethylene), four different particle populations can be compared. The comparison was carried out  
 417 at the three wavelengths (nearly) common to PAXs and MWAA (i.e.,  $\lambda = 870/850, 532$  and  $405$  nm). Fig 10  
 418 shows the comparison at  $\lambda = 870/850$  nm, while comparison at  $\lambda = 532$  and  $405$  nm are reported in  
 419 Supplementary (see Fig. S.6 and S.7, respectively). We divided the results by fuel, air flow and with/without  
 420 cyclone. Each point in the plots sums-up the observations at different global equivalence ratio values. All the  
 421 measured MAC values, including the other two wavelengths available for the MWAA (i.e.,  $635$  and  $375$  nm)  
 422 too, are summarized in Table 5.

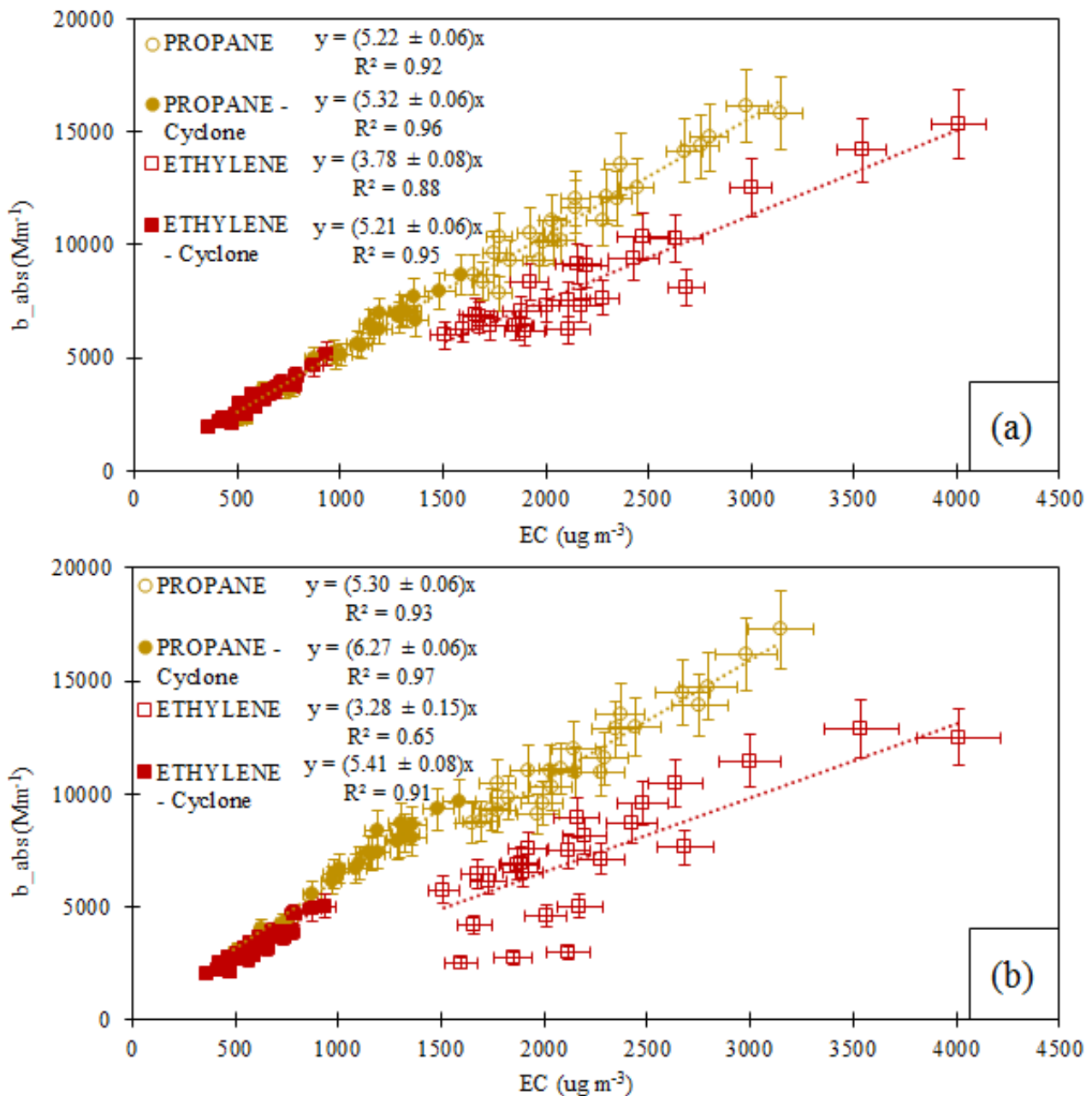
423 *Table 5: Summary of the measured MAC values, in  $m^2 g^{-1}$ .*

FUEL	PAX			MWAA				
	870 nm	532 nm	405 nm	850 nm	635 nm	532 nm	405 nm	375 nm
<b>PROPANE</b>	$5.30 \pm 0.06$	$8.35 \pm 0.08$	$10.55 \pm 0.11$	$5.22 \pm 0.06$	$7.22 \pm 0.09$	$8.81 \pm 0.09$	$10.55 \pm 0.09$	$10.86 \pm 0.12$
<b>PROPANE with cyclone</b>	$6.27 \pm 0.06$	$10.26 \pm 0.06$	$13.48 \pm 0.08$	$5.32 \pm 0.06$	$7.37 \pm 0.07$	$8.95 \pm 0.08$	$10.91 \pm 0.11$	$11.59 \pm 0.14$
<b>ETHYLENE</b>	$3.28 \pm 0.15$	$4.92 \pm 0.19$	$5.89 \pm 0.20$	$3.78 \pm 0.08$	$5.00 \pm 0.09$	$5.91 \pm 0.11$	$6.90 \pm 0.12$	$7.28 \pm 0.14$
<b>ETHYLENE with cyclone</b>	$5.41 \pm 0.08$	$10.42 \pm 0.12$	$15.74 \pm 0.15$	$5.21 \pm 0.06$	$7.62 \pm 0.07$	$9.53 \pm 0.08$	$12.29 \pm 0.10$	$13.03 \pm 0.11$

424

425 The MWAA analysis at  $\lambda = 870$  nm (Fig. 10.a) returned compatible MAC values for both propane series  
 426 (with/without cyclone) and ethylene series with cyclone, while a consistently lower MAC value was found for  
 427 the ethylene series (worse correlation) without the PM1 cutting. The same picture turned out at the other two  
 428 wavelengths (see Supplementary Fig. S.6 and S.7). By comparing PAX absorption coefficients and EC  
 429 concentrations at  $\lambda = 870$  nm (Fig. 10.b), obtained MAC values are more variable, with similar values only in  
 430 the case of propane without cyclone and ethylene with cyclone. At  $\lambda = 532$ , in the case of MWAA, similar  
 431 MAC values have been found for both the propane series, while, for ethylene series, MAC values were slightly  
 432 higher when cyclone was used and lower when not. Considering the optical data from PAX, a similar MAC  
 433 for both the fuels was found when the cyclone was present, while it slightly differed in the case of propane  
 434 without cyclone, and it was much lower in the case of ethylene without cyclone. At  $\lambda = 405$  nm, the MWAA  
 435 responses for propane series were still in agreement while the ethylene series showed a higher MAC value  
 436 when using the cyclone, and a lower MAC value without using it. PAX returned a different MAC value for  
 437 each of the four conditions. To summarize, if series with cyclone are only considered, MAC values show small  
 438 differences depending on the fuel, larger in the case of PAXs. The ethylene series without cyclone showed the  
 439 lowest MAC values of the whole data set: the most likely reason for this difference is the presence of super-  
 440 micrometric particles (see Sect 3.2.1 and Fig. 6) when the cyclone was not used. With MWAA, the MAC  
 441 values turned out to be the same in all the runs but the case of the ethylene data collected without the cyclone.  
 442 With the PAXs analysis, MAC values turned out higher in the series with cyclone, this happened at all the  
 443 three wavelengths and for both fuels. Since PAXs data showed a higher variability in MAC values,  
 444 photoacoustic measurements are supposed to be more sensitive to particle size than filter based MWAA  
 445 analysis.





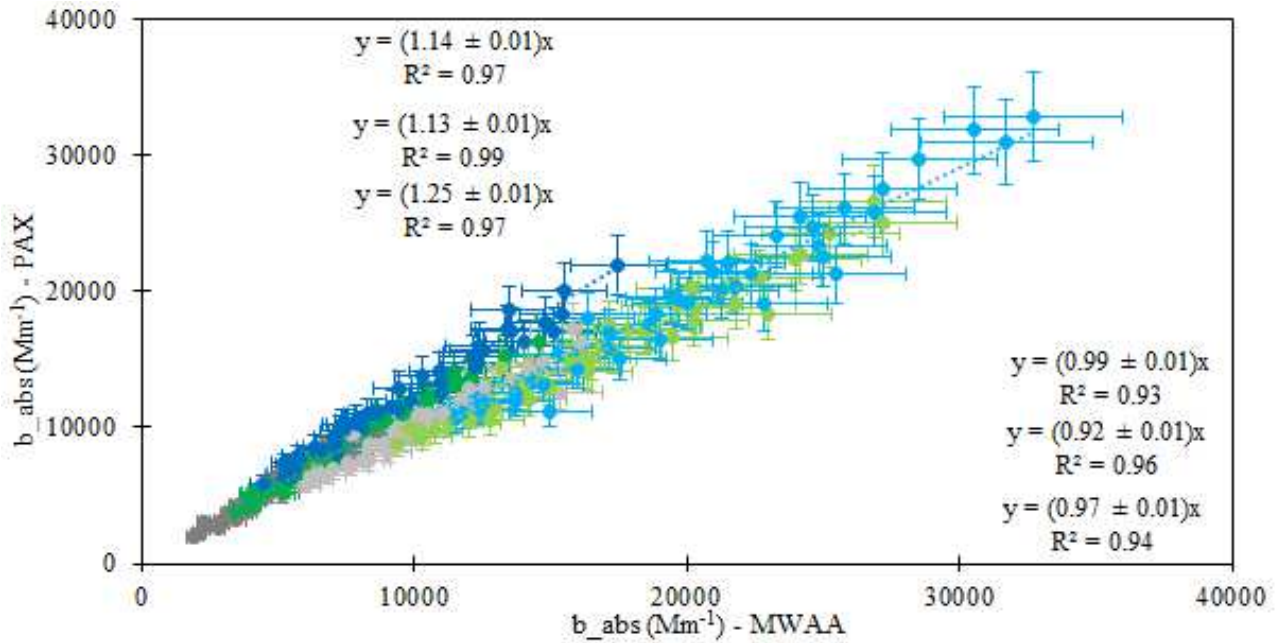
446

447 Figure 10: Absorption coefficient @850 nm measured by MWA (a) and @870 nm measured by PAX (b) versus EC  
 448 concentration. The slope of each fit corresponds to the Mass Absorption Coefficient.

449 MAC values are close to theoretical figures for soot (Bond and Bergstrom, 2006), for both the fuels and at all  
 450 the wavelengths. IR values are similar to those obtained by Moallemi (2019) for propane exhaust. With both  
 451 the fuels MAC values increase when super-micrometric particles were removed by the cyclone; propane-  
 452 particles showed higher MAC values than ethylene ones.

453 In (Moallemi et al., 2019), only IR-MAC values for propane are reported, resulting slightly lower than values  
 454 here quoted. This difference could depend on the techniques used to quantify the EC concentration: we  
 455 measured EC values by thermal optical analysis while Moallemi (2019) reported BC concentration measured  
 456 by LII.

457 Discrepancies between MAC values obtained by PAXs and MWA, for the same experiment, are  
 458 compatible with the differences of measured  $b_{abs}$  values: the latter are directly compared in Fig. 11, merging  
 459 all the data collected by the two setups (i.e., with and without the cyclone) and for the two fuels. The agreement  
 460 between the two instruments turned out within 25 % and 7 %, respectively without and with the cyclone.



461

462 *Figure 11: Correlation study between the absorption coefficient measured by PAX and MWAAs. Colours of dots identify*  
 463 *the wavelength of the analysis: grey refers to 870 nm, green to 532 nm and blue to 405 nm, with cyclone; light grey refers*  
 464 *to 870 nm, light green to 532 nm and light blue to 405 nm; without cyclone.*

465 In addition, the spectral dependence of the absorption coefficient  $b_{abs}$ , and consequently the Ångström  
 466 Absorption Exponent (AAE, Moosmüller et al., 2011), can be calculated by the power-law:

467 
$$b_{abs}(\lambda) \approx \lambda^{-AAE}$$

468 where:

- 469  $b_{abs}$  [ $Mm^{-1}$ ]: absorption coefficient
- 470  $\lambda$  [nm]: wavelength used for the analysis
- 471 AAE: Ångström Absorption Exponent.

472 The averages of the resulting AAEs values for the different experimental conditions are reported in Table 6 by  
 473 fitting the data for the 3 and 5 available wavelengths in the case of PAXs and MWAAs, respectively.

474 Experimental determinations of the AAE had been reported in the literature as being dependent on aerosol  
 475 chemical composition (Kirchstetter et al., 2004; Utry et al., 2013) and size and morphology (Lewis et al., 2008;  
 476 Lack et al., 2012; Lack and Langridge, 2013; Filep et al., 2013; Utry et al., 2014 a). Particulate generated by  
 477 fossil fuel combustion (i.e., Black Carbon) typically has AAE values close to 1.0 (Harrison et al., 2013, and  
 478 references therein). The AAE values measured in this work for the MISG exhausts are generally close to 1.0  
 479 with higher figures for the cyclone-selected aerosol.

480 *Table 6: AAE values obtained in different experimental conditions through the analysis of PAXs and MWAAs raw data.*

<b>EXPERIMENTAL CONDITIONS</b>	<b>AAE - PAX</b>	<b>AAE - MWAA</b>
<b>PROPANE 70 to 85 mlpm - AIR 7 lpm</b>	0.88 ± 0.06	0.92 ± 0.04
<b>PROPANE 70 to 85 mlpm - AIR 8 lpm</b>	0.92 ± 0.06	0.91 ± 0.05
<b>PROPANE 70 to 85 mlpm - AIR 7 lpm - cyclone</b>	0.98 ± 0.09	0.99 ± 0.10
<b>PROPANE 70 to 85 mlpm - AIR 8 lpm - cyclone</b>	1.05 ± 0.04	0.97 ± 0.09
<b>ETHYLENE 118 to 144 mlpm - AIR 7 lpm</b>	0.93 ± 0.28	0.84 ± 0.07
<b>ETHYLENE 118 to 144 mlpm - AIR 8 lpm</b>	0.76 ± 0.04	0.81 ± 0.06
<b>ETHYLENE 118 to 144 mlpm - AIR 7 lpm - cyclone</b>	1.40 ± 0.05	1.19 ± 0.09
<b>ETHYLENE 118 to 144 mlpm - AIR 8 lpm - cyclone</b>	1.39 ± 0.04	1.08 ± 0.05

481

482 Since the fit to 3 points could not be reliable, in the Supplementary (Table S.4) we reported the 2-wavelength  
483 calculations of the AAE for PAXs.

#### 484 **4. Conclusions**

485 A Mini-Inverted Soot Generator (MISG) was coupled with an atmospheric simulation chamber  
486 (ChAMBRe) to compare the emissions when the burner is fed by two different fuels, ethylene, and propane.  
487 Different combustion conditions (i.e., air and fuel flow, global equivalence ratio) were characterized in terms  
488 of size distribution, particle and gas composition, optical properties, and EC concentration in the exhausts.

489 The MISG turned out to be a stable and reproducible soot particles source, suitable for experiments in  
490 atmospheric simulation chambers. In addition, properties of emitted soot particles can be slightly modulated  
491 by varying the combustion conditions i.e., tuning the global equivalence ratio and/or varying the fuel used for  
492 combustion.

493 With equal conditions, ethylene combustion produced particles with higher number concentration and  
494 smaller diameter than propane. Anyway, particles generated by both the fuels were larger than the typical  
495 exhausts of modern engines, such as aircraft and diesel vehicle engines, which emit ultrafine soot particles.  
496 Furthermore, it is noteworthy that ethylene combustion also generates super-micrometric aggregates. These  
497 are likely formed in the stagnation plane at the bottom part of the combustion cell. This information should be  
498 kept in mind when planning experiments, since super-aggregates, if not desired, could affect analysis.

499 The carbonaceous compounds produced by propane are generally characterized by higher EC to TC ratios  
500 than ethylene.

501 From the optical point of view, particles generated by propane turned out to be more light absorbing than  
502 those formed by ethylene, although burning conditions (in terms of global equivalence ratio) were the same.  
503 The values of the MAC parameter show a substantial agreement except for those retrieved from the data  
504 collected in the ethylene-no cyclone experiments. The latter resulted in lower MAC values, probably due to  
505 the presence of super-aggregates in the chamber.

506 This work opens to new and more complex experiments. Well-characterized soot particles could be used to  
507 investigate the effects that atmospheric parameters such as temperature and relative humidity can have on soot  
508 particles, and to study the interactions between soot particles and gaseous pollutants, solar radiation or bio-  
509 aerosol.

#### 510 **Author contribution**

511 VV and DM prepared the experimental setup, performed all the experiments and the data analysis; DM, FP,  
512 SGD and PP designed and built ChAMBRe; MB designed and implemented the acquisition software; VV and  
513 DM prepared the article with contributions from the other authors.

#### 514 **Competing interests**

515 The authors declare that they have no conflict of interest.

## 516 **Special issue statement**

517 This article is part of the special issue “Simulation chambers as tools in atmospheric research  
518 (AMT/ACP/GMD inter-journal SI)”. It is not associated with a conference.

## 519 **Acknowledgments**

520 This project/work has received funding by the European Union’s Horizon 2020 research and innovation  
521 program through the EUROCHAMP-2020 Infrastructure Activity under grant agreement No 730997.

522 This project/work has received funding by MIUR through the PON project PIR\_00015 “Per ACTRIS IT”  
523 whose recipient is INFN.

## 524 **References**

525 Ackerman, A., Toon, O., Stevens, D., Heymsfield, A., Ramanathan, V., and Welton, E.: Reduction of tropical  
526 cloudiness by soot, *Science*, 288(5468), 1042–1047, doi:10.1126/science.288.5468.1042, 2000.

527 Anenberg, S. C., Horowitz, L. W., Tong, D. Q., and West, J. J.: An estimate of the global burden of  
528 anthropogenic ozone and fine particulate matter on premature human mortality using atmospheric modelling,  
529 *Environ. Health Perspec.*, 118 (9):1189–95, doi:10.1289/ehp.0901220, 2010.

530 Baccolo, G., Nastasi, M., Massabò, D., Clason, C., Di Mauro, B., Di Stefano, E., Łokas, E., Prati, P., Previtali,  
531 E., Takeuchi, N., Delmonte, B., Maggi, V.: Artificial and natural radionuclides in cryoconite as tracers of  
532 supraglacial dynamics: Insights from the Morteratsch glacier (Swiss Alps), *CATENA*, 191:104577,  
533 10.1016/j.catena.2020.104577, 2020.

534 Becker, K. H. (2006): Overview on the Development of Chambers for the Study of Atmospheric Chemical  
535 Processes, in: *Environmental Simulation Chambers: Application to Atmospheric Chemical Processes*, edited  
536 by: Barnes I. and Rudzinski K. J., Springer, Amsterdam, 1–26.

537 Bescond, A., Yon, J., Ouf, F. X., Roze, C., Coppalle, A., Parent, P., Ferry, D., and Laffon, C.: Soot optical  
538 properties determined by analyzing extinction spectra in the visible near-UV: Toward an optical speciation  
539 according to constituents and structure, *J. Aerosol Sci.* 101:118–32, doi:10.1016/j.jaerosci.2016.08.001, 2016.

540 Birch, M. E. and Cary, R. A.: Elemental carbon-based method for occupational monitoring of particulate diesel  
541 exhaust: methodology and exposure issues, *Analyst*, 121, 1183–1190, 1996.

542 Bischof, O. F., Weber, P., Bundke, U., Petzold, A., and Kiendler-Scharr, A.: Characterization of the  
543 Miniaturized Inverted Flame Burner as a Combustion Source to Generate a Nanoparticle Calibration Aerosol,  
544 *Emission Contr. Sci. Technol.* 6:37-46, DOI: 10.1007/s40825-019-00147-w, 2019.

545 Bond, T. C., and Bergstrom, R. W.: Light Absorption by Carbonaceous Particles: An Investigative Review,  
546 *Aerosol Science and Technology*, 40:1, 27-67, DOI: 10.1080/02786820500421521, 2006.

547 Bond T. C., Covert D. S., and Müller T.: Truncation and Angular-Scattering Corrections for Absorbing  
548 Aerosol in the TSI 3563 Nephelometer, *Aerosol Science and Technology*, 43:9, 866-871, DOI:  
549 10.1080/02786820902998373, 2009.

- 550 Bond, T. C., Doherty, S. J., Fahey, D. W., Forster, P. M., Berntsen, T., De Angelo, B. J., et al.: Bounding the  
551 role of black carbon in the climate system: A scientific assessment, *Journal of Geophysical Research*  
552 *Atmospheres*, 118(11), 5380–5552. <https://doi.org/10.1002/jgrd.50171>, 2013.
- 553 Caponi, L., Formenti, P., Massabó, D., Di Biagio, C., Cazaunau, M., Pangui, E., Chevaillier, S., Landrot, G.,  
554 Andreae, M. O., Kandler, K., Piketh, S., Saeed, T., Seibert, D., Williams, E., Balkanski, Y., Prati, P., and  
555 Doussin, J.-F.: Spectral- and size-resolved mass absorption efficiency of mineral dust aerosols in the shortwave  
556 spectrum: a simulation chamber study, *Atmos. Chem. Phys.*, 17, 7175–7191, <https://doi.org/10.5194/acp-17-7175-2017>, 2017.
- 558 Cassee, F. R., Héroux, M. E., Gerlofs-Nijland, M. E., and Kelly, F. J.: Particulate matter beyond mass: Recent  
559 health evidence on the role of fractions, chemical constituents and sources of emission, *Inhalation Toxicology*,  
560 25(14), 802–812. <https://doi.org/10.3109/08958378.2013.850127>, 2013.
- 561 Chakrabarty, R. K., Moosmüller, H., Garro, M. A., and Stipe, C. B.: Observation of Superaggregates from a  
562 Reversed Gravity Low-Sooting Flame, *Aerosol Science and Technology*, 46:1, i-iii, DOI:  
563 10.1080/02786826.2011.608389, 2012.
- 564 Cross, E. S., Onasch, T. B., Ahern, A., Wrobel, W., Slowik, J. G., Olfert, J., Lack, D. A., Massoli, P., Cappa,  
565 C. D., Schwarz, J. P., et al.: Soot particle studies-instrument inter-comparison-project overview, *Aerosol Sci.*  
566 *Technol.*, 44 (8):592–611. doi:10.1080/02786826.2010.482113, 2010.
- 567 Danelli, S. G., Brunoldi, M., Massabò, D., Parodi, F., Vernocchi, V., and Prati, P.: Comparative  
568 characterization of the performance of bio-aerosol nebulizers in connection with atmospheric simulation  
569 chambers, *Atmos. Meas. Tech.*, 14, 4461–4470, <https://doi.org/10.5194/amt-14-4461-2021>, 2021.
- 570 Durdina, L., Lobo, P., Trueblood, M. B., Black, E. A., Achterberg, S., Hagen, D. E., Brem, B. T., and Wang,  
571 J.: Response of real-time black carbon mass instruments to mini-CAST soot, *Aerosol Sci. Technol.* 50 (9):  
572 906–18, doi: 10.1080/02786826.2016.1204423, 2016.
- 573 Filep, Á., Ajtai, T., Utry, N., Pintér, M. D., Nyilas, T., Takács, S., Máté, Z., Gelencsér, A., Hoffer, A.,  
574 Schnaiter, M., Bozóki, Z., and Szabó, G.: Absorption spectrum of ambient aerosol and its correlation with size  
575 distribution in specific atmospheric conditions after a red mud accident, *Aerosol Air Qual. Res.*, 13, 49–59,  
576 2013.
- 577 Finlayson-Pitts, B. J. and Pitts Jr., J. N.: *Chemistry of the upper and lower atmosphere: Theory, experiments*  
578 *and applications*, Academic Press, San Diego, CA, 2000.
- 579 Gan, W. Q., Koehoorn, M., Davies, H. W., Demers, P. A., Tamburic, L., and Brauer, M.: Long-term exposure  
580 to traffic-related air pollution and the risk of coronary heart disease hospitalization and mortality,  
581 *Environmental Health Perspectives*, 119(4), 501–507, <https://doi.org/10.1289/ehp.1002511>, 2011.
- 582 Ghazi, R., and Olfert, J. S.: Coating mass dependence of soot aggregate restructuring due to coatings of oleic  
583 acid and dioctyl sebacate, *Aerosol Sci. Technol.* 47 (2):192–200. doi:10.1080/02786826.2012.741273, 2013.
- 584 Ghazi, R., Tjong, H., Soewono, A., Rogak, S. N., and Olfert, J. S.: Mass, mobility, volatility, and morphology  
585 of soot particles generated by a McKenna and inverted burner, *Aerosol Sci. Technol.* 47 (4):395–405.  
586 doi:10.1080/02786826.2012.755259, 2013.
- 587 Harrison, R. M., Beddows, D. C. S., Jones A. M., Calvo A., Alves C., and Pio C.: An evaluation of some issues  
588 regarding the use of aethalometers to measure woodsmoke concentrations, *Atmos. Environ.*, 80, 540–548,  
589 2013.

590 Henning, S., Ziese, M., Kiselev, A., Saathoff, H., Möhler, O., Mentel, T. F., Buchholz, A., Spindler, C.,  
591 Michaud, V., Monier, M., et al.: Hygroscopic growth and droplet activation of soot particles: Uncoated,  
592 succinic or sulfuric acid coated, *Atmos. Chem. Phys.* 12 (10):4525–37. doi: 10.5194/acp-12-4525-2012, 2012.

593 Hu, D., Alfarra, M. R., Szpek, K., Langridge, J. M., Cotterell, M. I., Belcher, C., Rule, I., Liu, Z., Yu, C., Shao,  
594 Y., Voliotis, A., Du, M., Smith, B., Smallwood, G., Lobo, P., Liu, D., Haywood, J. M., Coe, H., and Allan, J.  
595 D.: Physical and chemical properties of black carbon and organic matter from different combustion and  
596 photochemical sources using aerodynamic aerosol classification, *Atmos. Chem. Phys.*, 21, 16161–16182,  
597 <https://doi.org/10.5194/acp-21-16161-2021>, 2021.

598 Janssen, N., Gerlofs-Nijland, M., Lanki, T., Salonen, R., Cassee, F., Hoek, G., Fischer, P., Brunekreef, B., and  
599 Krzyzanowski, M.: Health effects of black carbon, Res. Rep., World Health Organization, Regional Office for  
600 Europe, Copenhagen, Denmark, 2012

601 Kazemimanesh, M., Moallemi, A., Thomson, K., Smallwood, G., Lobo, P., and Olfert, J. S.: A novel miniature  
602 inverted-flame burner for the generation of soot nanoparticles, *Aerosol Science and Technology*, 53 (2), 184-  
603 195, [10.1080/02786826.2018.1556774](https://doi.org/10.1080/02786826.2018.1556774), 2019.

604 Kirchstetter, T. W., Novakok, T., and Hobbs, P. V.: Evidence that the spectral dependence of light absorption  
605 by aerosols is affected by organic carbon, *J. Geophys. Res.*, 109, D21208,  
606 <https://doi.org/10.1029/2004JD004999>, 2004.

607 Kumar, N. K., Corbin, J. C., Bruns, E. A., Massabó, D., Slowik, J. G., Drinovec, L., Močnik, G., Prati, P.,  
608 Vlachou, A., Baltensperger, U., Gysel, M., El-Haddad, I., and Prévôt, A. S. H.: Production of particulate brown  
609 carbon during atmospheric aging of residential wood-burning emissions, *Atmos. Chem. Phys.*, 18, 17843–  
610 17861, <https://doi.org/10.5194/acp-18-17843-2018>, 2018.

611 Lack, D. A. and Langridge, J. M.: On the attribution of black and brown carbon light absorption using the  
612 Ångström exponent, *Atmos. Chem. Phys.*, 13, 10535–10543, <https://doi.org/10.5194/acp-13-10535-2013>,  
613 2013.

614 Lack, D. A., Langridge, J. M., Bahreini, R., Cappa, C. D., Middlebrook, A. M., and Schwarz, J. P.: Brown  
615 carbon and internal mixing in biomass burning particles, *P. Natl. Acad. Sci. USA*, 109, 14802–14807, 2012.

616 Lelieveld, J., Evans, J. S., Fnais, M., Giannadaki, D., and Pozzer, A.: The contribution of outdoor air pollution  
617 sources to premature mortality on a global scale, *Nature* 525 (7569):367–71. doi:10.1038/nature15371, 2015.

618 Lewis, K., Arnott, W. P., Moosmüller, H., and Wold, C. E.: Strong spectral variation of biomass smoke light  
619 absorption and single scattering albedo observed with a novel dual-wavelength photoacoustic instrument, *J.*  
620 *Geophys. Res.*, 113, D16203, <https://doi.org/10.1029/2007JD009699>, 2008.

621 Mamakos, A., Khalek, I., Giannelli, R., and Spears, M.: Characterization of Combustion Aerosol Produced by  
622 a Mini-CAST and Treated in a Catalytic Stripper, *Aerosol Science and Technology*, 47:8, 927-936,  
623 DOI:10.1080/02786826.2013.802762, 2013.

624 Massabò, D., and Prati P.: An overview of optical and thermal methods for the characterization of  
625 carbonaceous aerosol, *La Rivista del Nuovo Cimento*, vo. 44:3, DOI: 10.1007/s40766-021-00017-8, 2021.

626 Massabò, D., Prati, P., Canepa, E., Bastianini, M., Van Eijk, A.M.J., Missamou, T., Piazzola, J.:  
627 Characterization of carbonaceous aerosols over the Northern Adriatic Sea in the JERICO-NEXT project  
628 framework, *Atmospheric Environment*, 228:117449, DOI: 10.1016/j.atmosenv.2020.117449, 2020.

- 629 Massabò, D., Altomari, A., Vernocchi, V., and Prati, P.: Two-wavelength thermal–optical determination of  
630 light-absorbing carbon in atmospheric aerosols, *Atmos. Meas. Tech.*, 12, 3173–3182,  
631 <https://doi.org/10.5194/amt-12-3173-2019>, 2019.
- 632 Massabò, D., Danelli S. G., Brotto P., Comite A., Costa C., Di Cesare A., Doussin J. F., Ferraro F., Formenti  
633 P., Gatta E., Negretti L., Oliva M., Parodi F., Vezzulli L., and Prati P.: ChAMBRé: a new atmospheric  
634 simulation chamber for aerosol modelling and bioaerosol research, *Atmos. Meas. Tech.* 11, 5885-5900, 2018.
- 635 Massabò, D., Caponi, L., Bove, M. C., and Prati, P.: Brown carbon and thermal-optical analysis: a correction  
636 based on optical multiwavelength apportionment of atmospheric aerosols, *Atmos. Environ.*, 125, 119–125,  
637 <https://doi.org/10.1016/j.atmosenv.2015.11.011>, 2016.
- 638 Massabò, D., Caponi, L., Bernardoni, V., Bove, M. C., Brotto, P., Calzolari, G., Cassola, F., Chiari, M., Fedi,  
639 M. E., Fermo, P., Giannoni, M., Lucarelli, F., Nava, S., Piazzalunga, A., Valli, G., Vecchi, R., and Prati, P.:  
640 Multi-wavelength optical determination of black and brown carbon in atmospheric aerosols, *Atmos. Environ.*,  
641 108, 1–12, 2015.
- 642 Menon, S., Hansen, J., Nazarenko, L., and Luo, Y.: Climate effects of black carbon aerosols in China and  
643 India, *Science* 297 (5590):2250–53. doi:10.1126/science1075159, 2002.
- 644 Moallemi, A., Kazemimanesh, M., Corbin, J. C., Thomson, K., Smallwood, G., Olfert, J. S., and Lobo, P.:  
645 Characterization of black carbon particles generated by a propane-fueled miniature inverted soot generator,  
646 *Journal of Aerosol Science*, 135, 46-57, 10.1016/j.jaerosci.2019.05.004, 2019.
- 647 Modini, R. L., Corbin, J. C., Brem, B. T., Irwin, M., Bertò, M., Pileci, R. E., Fetfatzis, P., Eleftheriadis, K.,  
648 Henzing, B., Moerman, M. M., Liu, F., Müller, T., and Gysel-Beer, M.: Detailed characterization of the CAPS  
649 single-scattering albedo monitor (CAPS PM<sub>ss</sub>a) as a field-deployable instrument for measuring aerosol light  
650 absorption with the extinction-minus-scattering method, *Atmos. Meas. Tech.*, 14, 819–851,  
651 <https://doi.org/10.5194/amt-14-819-2021>, 2021.
- 652 Moore R. H., Ziemba L. D., Dutcher D., Beyersdorf A. J., Chan K., Crumeyrolle S., Raymond T. M., Thornhill  
653 K. L., Winstead E. L. and Anderson B. E.: Mapping the Operation of the Miniature Combustion Aerosol  
654 Standard (Mini-CAST) Soot Generator, *Aerosol Science and Technology*, 48:5, 467-479, DOI:  
655 10.1080/02786826.2014.890694, 2014.
- 656 Moosmüller, H., Chakrabarty, R.K., Ehlers, K.M., Arnott, W.P.: Absorption Ångström coefficient, brown  
657 carbon, and aerosols: basic concepts, bulk matter, and spherical particles. *Atmos. Chem. Phys.* 11, 1217e1225,  
658 2011.
- 659 Moschos, V., Gysel-Beer, M., Modini, R. L., Corbin, J. C., Massabò, D., Costa, C., Danelli, S. G., Vlachou,  
660 A., Daellenbach, K. R., Szidat, S., Prati, P., Prévôt, A. S. H., Baltensperger, U., and El Haddad, I.: Source-  
661 specific light absorption by carbonaceous components in the complex aerosol matrix from yearly filter-based  
662 measurements, *Atmos. Chem. Phys.*, 21, 12809–12833, <https://doi.org/10.5194/acp-21-12809-2021>, 2021.
- 663 Nemmar, A., Hoet, P.H.M., Vanquickenborne, B., Dinsdale, D., Thomeer, M., Hoylaerts, M.F., Vanbilloen,  
664 H., Mortelmans, L., Nemery, B.: Passage of inhaled particles into the blood circulation in humans. *Circulation*  
665 105, 411–414, <https://doi.org/10.1161/hc0402.104118>, 2002.
- 666 Nienow, A.M., and Roberts, J.T.: Heterogeneous Chemistry of Carbon Aerosols. *Annual Review of Physical*  
667 *Chemistry* 57, 105–128, <https://doi.org/10.1146/annurev.physchem.57.032905.104525>, 2006.

- 668 NIOSH: Method 5040 Issue 3: Elemental Carbon (Diesel Exhaust). In NIOSH Manual of Analytical Methods.  
669 National Institute of Occupational Safety and Health, Cincinnati, OH, 1999.
- 670 Nordmann, S., Birmili, W., Weinhold, K., Müller, K., Spindler, G., and Wiedensohler, A.: Measurements of  
671 the mass absorption cross section of atmospheric soot particles using Raman spectroscopy, *J. Geophys. Res.*  
672 *Atmos.*, 118, 12,075–12,085, doi: 10.1002/2013JD020021, 2013.
- 673 Oberdörster, G., Oberdörster, E., Oberdörster, J.: Nanotoxicology: An Emerging Discipline Evolving from  
674 Studies of Ultrafine Particles, *Environmental Health Perspectives* 113, 823–839.  
675 <https://doi.org/10.1289/ehp.7339>, 2005.
- 676 Onasch, T. B., Trimborn, A., Fortner, E. C., Jayne, J. T., Kok, G. L., Williams, L. R., Davidovits, P. and  
677 Worsnop, D. R.: Soot particle aerosol mass spectrometer: Development, validation, and initial application,  
678 *Aerosol Sci. Technol.* 46 (7):804–17, doi:10.1080/02786826.2012.663948, 2012.
- 679 Pagels, J., Khalizov, A. F., McMurry, P. H., and Zhang, R. Y.: Processing of soot by controlled sulphuric acid  
680 and water condensation—Mass and mobility relationship, *Aerosol Sci. Technol.* 43 (7):629–4,  
681 doi:10.1080/02786820902810685, 2009.
- 682 Petzold, A., Ogren, J. A., Fiebig, M., Laj, P., Li, S.-M., Baltensperger, U., Holzer-Popp, T., Kinne, S.,  
683 Pappalardo, G., Sugimoto, N., Wehrli, C., Wiedensohler, A., and Zhang, X.-Y.: Recommendations for  
684 Reporting “Black Carbon”, *Measurements. Atmos. Chem. Phys.*, 13:8365–8379, 2013.
- 685 Petzold, A., Schloesser, H., Sheridan, P.J., Arnott, W.P., Ogren, J.A., Virkkula, A.: Evaluation of multiangle  
686 absorption photometry for measuring aerosol light absorption, *Aerosol Sci. Technol.* 39 (1), 2005.
- 687 Petzold, A., and Schöllner, M.: Multi-angle absorption photometry—a new method for the measurement of  
688 aerosol light absorption and atmospheric black carbon, *Journal of Aerosol Science*, 35, 421–441, 2004.
- 689 Pope, C.A. III, Burnett, R. T., Thun, M. J., Calle, E. E., Krewski, D., Ito, K., et al.: Lung Cancer,  
690 Cardiopulmonary Mortality, and Long-term Exposure to Fine Particulate Air Pollution. *J. Am. Med. Assoc.*,  
691 287(9):1132–41, 2002.
- 692 Quinn, P. K., Bates, T. S., Baum, E., Doubleday, N., Fiore, A. M., Flanner, M., et al.: Short-lived pollutants in  
693 the Arctic: Their climate impact and possible mitigation strategies, *Atmospheric Chemistry and Physics*, 8(6),  
694 1723–1735. <https://doi.org/10.5194/acp-8-1723-2008>, 2008.
- 695 Ramanathan, V., and G. Carmichael, G.: Global and regional climate changes due to black carbon, *Nat. Geosci.*  
696 1 (4):221–27. doi:10.1038/ngeo156, 2008.
- 697 Saturno, J., Pöhlker, C., Massabò, D., Brito, J., Carbone, S., Cheng, Y., Chi, X., Ditas, F., Hrabě de Angelis,  
698 I., Morán-Zuloaga, D., Pöhlker, M. L., Rizzo, L. V., Walter, D., Wang, Q., Artaxo, P., Prati, P., and Andreae,  
699 M. O.: Comparison of different Aethalometer correction schemes and a reference multi-wavelength absorption  
700 technique for ambient aerosol data, *Atmos. Meas. Tech.*, 10, 2837–2850, [https://doi.org/10.5194/amt-10-2837-](https://doi.org/10.5194/amt-10-2837-2017)  
701 2017, 2017.
- 702 Scerri, M. M., Kandler, K., Weinbruch, S., Yubero, E., Galindo N., Prati, P., Caponi, L., and Massabò, D.:  
703 Estimation of the contributions of the sources driving PM<sub>2.5</sub> levels in a Central Mediterranean coastal town,  
704 *Chemosphere*, 211, 465–481, <https://doi.org/10.1016/j.chemosphere.2018.07.104>, 2018.
- 705 Skiles, S.M., Flanner, M., Cook, J.M., Dumont, M., Painter, T.H.: Radiative forcing by light-absorbing  
706 particles in snow. *Nature Clim Change* 8, 964–971. <https://doi.org/10.1038/s41558-018-0296-5>, 2018.



- 707 Stipe, C. B., Higgins, B. S., Lucas, D., Koshland, C. P., & Sawyer, R. F. Inverted co-flow diffusion flame for  
708 producing soot, *Review of Scientific Instruments*, 76 (2), <https://doi.org/10.1063/1.1851492>, 2005.
- 709 Utry, N., Ajtai, T., Filep, Á., Dániel P. M., Hoffer, A., Bozoki, Z., and Szabó, G.: Mass specific optical  
710 absorption coefficient of HULIS aerosol measured by a four-wavelength photoacoustic spectrometer at NIR,  
711 VIS and UV wavelengths, *Atmos. Environ.*, 69, 321–324, 2013.
- 712 Utry, N., Ajtai, T., Filep, Á., Pintér, M., Török, Zs., Bozóki, Z., and Szabó, G.: Correlations between absorption  
713 Angström exponent (AAE) of wintertime ambient urban aerosol and its physical and chemical properties,  
714 *Atmos. Environ.*, 91, 52–59, 2014.
- 715 Utry, N., Ajtai, T., Pinter, M., Bozóki, Z., and Szabó, G.: Wavelength-dependent optical absorption properties  
716 of artificial and atmospheric aerosol measured by a multiwavelength photoacoustic spectrometer. *Int. J.*  
717 *Thermophys.*, 35 (12):2246–58. doi:10.1007/s10765-014-1746-6, 2014
- 718 von der Weiden, S.-L., Drewnick, F., and Borrmann, S.: Particle Loss Calculator – a new software tool for the  
719 assessment of the performance of aerosol inlet systems, *Atmos. Meas. Tech.*, 2, 479–494,  
720 <https://doi.org/10.5194/amt-2-479-2009>, 2009.
- 721 Weijer, E. P., Schaap, M., Nguyen, L., Matthijsen, J., Denier van der Gon, H. A. C., et al.: Anthropogenic and  
722 Natural Constituents in Particulate Matter in the Netherlands, *Atmos. Chem. Phys.*, 11:2281–2294, 2011.
- 723 Zhang, R., Khalizov, A. F., Pagels, J., Zhang, D., Xue, H., and McMurry, P. H.: Variability in morphology,  
724 hygroscopicity, and optical properties of soot aerosols during atmospheric processing, *Proc. Natl. Acad. Sci.*  
725 *USA* 105 (30):10291–96. doi:10.1073/pnas.0804860105, 2008.